Dalton Transactions

ROYAL SOCIETY OF CHEMISTRY

PERSPECTIVE

View Article Online
View Journal | View Issue

Cite this: *Dalton Trans.*, 2024, **53**, 13280

Colloidal synthesis of two-dimensional nanocrystals by the polyol route

Tanner Q. Kimberly, Michelle H. Frasch and Susan M. Kauzlarich *

Received 4th May 2024,
Accepted 17th July 2024

DOI: 10.1039/d4dt01322k

rsc.li/dalton

The field of 2D nanomaterials is ever-growing with a myriad of synthetic advancements that have been used to obtain such materials. There are top-down, as well as bottom-up, fabrication methods for obtaining 2D nanomaterials; however, synthesis of 2D nanomaterials from solution offers a simple scalable way to control size, shape, and surface. This review outlines the recent advances in colloidal polyol synthesis of 2D nanomaterials and provides perspectives on the similarities and differences in various syntheses. Various materials classes are presented and discussed, including metals, oxides, chalcogenides, and halides, that can be synthesized as 2D nanomaterials *via* a polyol process. Throughout the literature, polyol media is demonstrated to be versatile not only as a solvent and reducing agent for metal precursors but also as a binding and shape-directing agent for many 2D nanomaterials. Polyols also offer the ability to dissolve various surfactants and additives that can further control the morphology and composition of various nanomaterials. In this review, we outline the various 2D materials that have been realized *via* the solution polyol route.

1. Introduction

Two-dimensional (2D) nanocrystals are anisotropic materials with nanometer scale thickness and large lateral dimensions. Since the realization of graphene,[1] which was obtained *via* mechanical exfoliation of graphite with scotch-tape, the field of 2D nanomaterials has seen an explosion of activity due to their interesting chemical, physical, and mechanical properties.[2–4] Many 2D nanocrystals are layered structures, such as transition metal dichalcogenides (TMDs), tetradymites, layered double hydroxides (LDHs), and others, which is the thermodynamic driving force for 2D growth, featuring covalent bonding within the layers and weak van der Waals forces between layers.[5–8] However, there are many reports of 2D nanocrystals synthesized from non-layered structures, such as face-centered cubic (fcc) metals,[9–11] wurtzite,[12,13] and rock-salt structures[14] for example. Recent developments in synthetic techniques have allowed for the realization of various 2D nanocrystals with a range of promising applications from optoelectronics to thermoelectrics.[15–17]

There are a variety of synthetic methods employed to obtain 2D nanocrystals, including exfoliation of bulk phases into thinner nanosheets,[18–21] chemical vapor deposition,[22,23] physical vapor deposition,[24–26] solution route synthetic processes,[27,28] and other methods.[29–31] Exfoliation is a widely employed and relatively straightforward method for obtaining 2D nanocrystalline materials.[32–34] Chemical deposition methods, like vapor–liquid–solid (VLS) growth, have been successfully employed in the synthesis of GaSe,[35] In_2Se_3,[36] and Bi_2Te_3/Bi_2Se_3 heterostructures.[37] Physical deposition methods, such as molecular beam epitaxy (MBE), have also allowed for the realization of highly crystalline and highly oriented nanoplates of InAs,[38] Bi_2Te_3,[39] and $MoSe_2$.[40] Another very powerful synthetic technique, due to its versatility and precise control over size, morphology, and composition, is solution-route colloidal synthesis, which has been largely employed in the preparation of 2D nanomaterials.[41–46]

Although there are numerous reports on the bottom-up colloidal synthesis of 2D nanocrystals, there are a very limited number that utilize the polyol process. Polyols are of particular importance in the field of nanocrystal synthesis because they are green solvents that have a large range in boiling points, due to their variable polymer lengths (*i.e.* ethylene glycol, diethylene glycol, triethylene glycol, *etc.*) and comparable reagent solubility to other commonly employed alkylamines or organophosphines. The term "polyol process" was first coined in 1988 by Fievet *et al.*,[47] where polyol solvents were used to synthesize metallic particles, and has since been expanded to various other materials classes.[48] This solution route synthetic technique utilizes polyols as both the solvent and reducing agent for metal salt precursors. The redox mechanism for polyols has been extensively studied, and it is established that the first oxidized product of ethylene glycol is glycolaldehyde, and subsequent oxidation yields CO_2, as described in

Department of Chemistry, University of California, One Shields Avenue, Davis, California 95616, USA. E-mail: smkauzlarich@ucdavis.edu

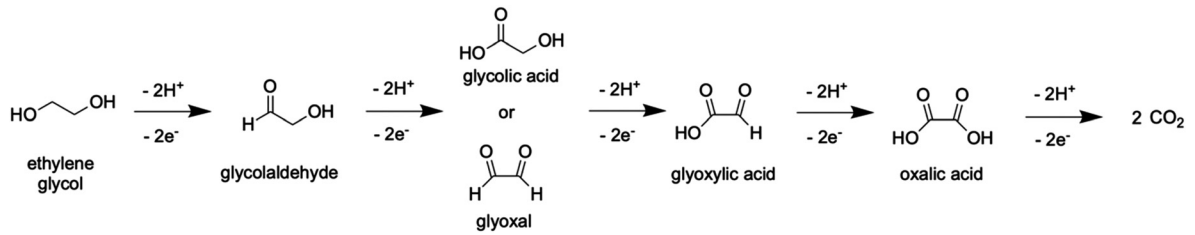

Scheme 1 The stepwise oxidation of ethylene glycol to yield CO_2. Adapted from ref. 48. Copyright 2018 Royal Society of Chemistry.

Scheme 1.[49,50] Utilizing polyols as reducing agents allows for conversion of metal salt precursors into a diverse array of materials and structure types with a high degree of synthetic tunability. Although there are many reports on the polyol synthesis of nanoparticles to-date, there are a limited number of papers on 2D morphologies obtained *via* this method.

In this review, we discuss various classes of materials that have been synthesized as 2D nanocrystals *via* a polyol process: including 2D metal, oxide, chalcogenide, and halide nanocrystals. Polyol solvents have the extraordinary ability to act as coordinating solvents with a large range of boiling points, enabling kinetic and thermodynamic control over many 2D nanostructures. Furthermore, polyol media is highly compatible with various inorganic salt precursors and surfactants, which enables a breadth of 2D materials syntheses. The polyol process is a powerful synthetic technique that allows for the realization of various 2D nanocrystals with a myriad of structures and compositions.

2. Metals

The most ubiquitous family of 2D nanocrystals that have been synthesized *via* the polyol route are mostly noble metals, such as gold[51–56] and silver,[57–59] and some other metalloids and alloys,[60,61] as described in Table 1. Many of these 2D metal nanomaterials are investigated for their surface plasmon resonances or potential catalytic activity. There are numerous reports on the synthesis of gold nanoplates using polyols. Most synthesis typically employ $HAuCl_4$ as the gold precursor with varying amounts of polyvinylpyrrolidone (PVP) dissolved in ethylene glycol (EG) or diethylene glycol (DEG) and heated at various temperatures and times. Kan *et al.* report the synthesis of gold nanoplates *via* a polyol process, shown in Fig. 1, and observe a 2D shape directing effect when PVP is used in tandem with EG, but not in aqueous conditions.[62] This anisotropic growth is attributed to the preference of PVP and EG to bind to the (111) planes of the gold nuclei and promote growth along the ⟨110⟩ direction, thus yielding 2D structures. By extending the reaction time from 5 to 40 minutes, they were able to obtain nanoplates with smaller and larger lateral dimensions as shown in Fig. 1a and b, respectively. This growth directing effect was also observed in other gold nanoplates synthesized *via* polyol processes.[52,53]

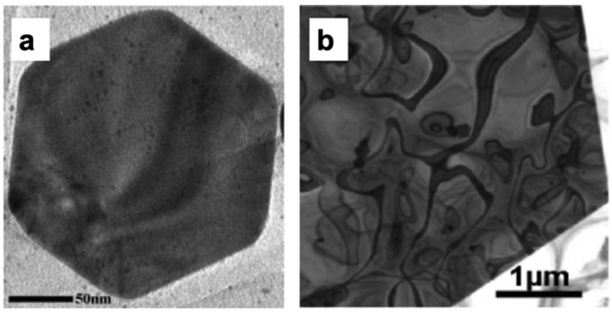

Fig. 1 TEM images of (a) smaller gold nanoplate synthesized at 5 min and (b) larger gold nanoplate synthesized at 40 min. Adapted with permission from ref. 62. Copyright 2006 American Chemical Society.

In a study by Xiong, *et al.*, palladium nanoplates were synthesized by a polyol process, as shown in Fig. 2, in an effort to explore their surface plasmon resonance properties.[63] In their synthesis, Na_2PdCl_4 was used as the palladium precursor and they observed that the 2D nanoplate morphology was strongly dependent on the exact ratio of PVP to Na_2PdCl_4. At low precursor concentrations, the reduction kinetics are slow enough that the thermodynamically stable morphology, which is cubooctahedra, is avoided and the 2D nanoplate morphology is kinetically stabilized in the presence of PVP as shown in Fig. 2a and b. Through electron diffraction studies they observed that the basal nanoplate planes were terminated at the (111) planes and the edges were the (100) facets, which is shown in the schematic inset of Fig. 2c. They confirm the lattice spacing of the forbidden 1/3(422) reflection to be 2.4 Å, in agreement with the palladium fcc lattice, as shown in Fig. 2d. These observations imply a similar mechanism whereby the PVP polymer binds preferentially to the (111) planes to promote 2D growth.

Other noble metal 2D nanocrystals have been synthesized in polyol media, including 2D rhodium nanoplates, which

Table 1 Metal nanomaterials synthesized with 2D morphology *via* a polyol process

Material	Morphology	Structure	Ref.
Ag	Nanoplates	fcc	57–59
Au	Nanoplates	fcc	51–56 and 62
BiRh	Nanoplates	fcc	60
Bi	Nanoplates	fcc	61
Pd	Nanoplates	fcc	63
Rh	Nanoplates	fcc	64

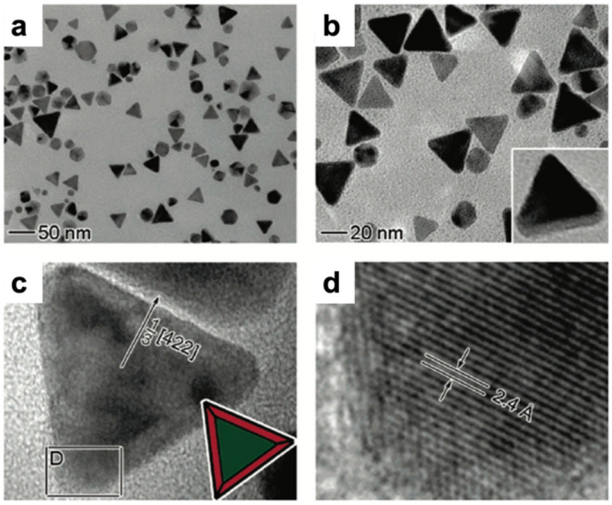

Fig. 2 (a) Low magnification and (b) high magnification TEM images of palladium nanoplates; inset in (b) shows a tilted nanoplate. (c) HRTEM of palladium nanoplate; the inset shows a cartoon schematic of the palladium nanoplate with (111) in green and (100) in red. (d) HRTEM of edge of nanoplate with lattice spacing of 2.4 Å. Adapted with permission from ref. 63. Copyright 2005 American Chemical Society.

were investigated for their catalytic activity.[64] In this synthesis, $Rh(acac)_3$ (acac = acetylacetonate) served as the rhodium precursor in 1,4-butandiol as the solvent and reducing agent. The slow dissolution of rhodium(III) ions from the acac ligands allowed for kinetic control over the rhodium nanocrystals, yielding hexagonal nanoplates at 225 °C in the presence of PVP. It was also found that the hexagonal nanoplate morphology was strongly dependent on the PVP to rhodium ratio, as in the case of other metallic nanoplate syntheses.[62,63] Additionally, the high boiling point of the 1,4-butanediol enabled a systematic study of the effect of temperature on the rhodium nanoplate reaction, which concluded that higher temperatures yielded more monodisperse nanoplates. This kinetically limited growth at elevated temperatures in the presence of PVP enabled the selective growth direction for these rhodium nanoplates to be in the ⟨110⟩ direction, leaving the (111) planes exposed as the basal planes.

The synthesis of 2D nanoplates of bismuth has also been reported *via* a polyol process.[61] In this synthesis, the researchers utilized $NaBiO_3$ as the precursor and EG as the reducing agent and solvent in the presence of a large molecular weight PVP (1 300 000 MW). When the ratio of bismuth precursor to PVP was tuned precisely, 2D nanoplates were obtained from the reaction, as observed with the other previously discussed metals.[62–64] Through this synthetic process, a kinetically mediated shape control mechanism is proposed, in which the reduction of precursors to form the 2D bismuth nanoplates is kinetically hindered by the PVP capping agent, thus allowing 2D shape control. It was found that when the PVP to bismuth ratio was tuned to 0.8, triangular 2D nanoplates of bismuth were obtained, and if the ratio was lowered or increased, only spherical bismuth nanoparticles were obtained. When no PVP was present, the spherical bismuth nanoparticles had a large distribution in size, suggesting that there is insufficient stabilization of the particles during growth, and leads to aggregation. However, when the PVP to bismuth ratio was 5 or higher, spherical, monodisperse particles were obtained due to high coverage of PVP on the surface. This study demonstrates the versatility of the polyol solvent to yield desired 2D shapes with variability of capping agent and precursor ratios, ultimately allowing kinetically controlled growth of nanostructures.

For many 2D metal nanomaterials, it is proposed that EG will preferentially bind to the (111) facet through the lone-pair electrons of oxygen moieties.[65] Theoretical studies in the framework of density functional theory (DFT) have established that binding of EG, and other polyols such as glycerol, to the (111) surface of metals like Pd, Pt, Ni, and Cu, is thermodynamically favorable with negative binding energies.[66,67] It is reasonable that the ability of EG to preferentially bind to (111) facets of metal nanomaterials, in tandem with PVP, allows the directed growth of 2D materials through the exchange of surface ligands.

3. Oxides

Another group of materials that have been recently synthesized *via* the polyol process are 2D oxide nanocrystals, which are summarized in Table 2. Most oxide nanocrystals with 2D morphology that have been synthesized *via* polyol processes are typically limited to binary transition metal oxides like iron,[68,69] zinc,[70] and manganese oxides.[71] Although there are reports of more complex quaternary 2D phosphates such as $LiFePO_4$ and $LiMnPO_4$.[72,73] All of these polyol syntheses are surfactant-free and rely solely on the ion coordination and shape directing effects of the polyol solvents themselves.

Many of the polyol syntheses of 2D transition metal oxide nanocrystals employ ethylene glycol (EG), diethylene glycol (DEG), or a polyethylene glycol (PEG) as the coordinating solvent and shape directing agents.[70,71] For example, in the case of Fe_2O_3 nanoplates synthesis reported by Hao *et al.*, they

Table 2 Oxide nanomaterials synthesized with 2D morphology *via* a polyol process

Material	Morphology	Structure	Ref.
Fe_2O_3	Nanoplates	Rhombohedral (hematite)	68
$CuFe_2O_4/Fe_2O_3$	Porous nanoplates	Cubic/ rhombohedral	69
ZnO	Nanoplates from nanoparticles	Hexagonal (wurtzite)	70
Mn_2O_3	Nanoplates	Orthorhombic	71
Mn_3O_4	Nanoplates	Tetragonal (hausmannite)	71
$LiFePO_4$	Nanoplates	Orthorhombic	72
$LiMnPO_4$	Nanoplates	Orthorhombic	73
$LiNi_{1/3}Mn_{1/3}Co_{1/3}O_3$	Nanoplates	Hexagonal (α-$NaFeO_2$)	74
CoO	Nanoplates	Cubic	75

investigated the solvent effects of various polyols, alcohols, and water. They observed that the best 2D shape directing effect was achieved with polyols and alcohols, while water yielded only nanoparticles. Although alcohols enabled the successful synthesis of 2D hematite nanoplates in this study, smaller nanoparticles were also present. The authors of this study attribute the formation of small nanoparticles to the fast decomposition of the iron precursor in water compared to that of the polyols. The most selective solvent for 2D nanoplate morphology of hematite was found to be the PEGs. The authors found that these hematite nanoplates had high photocatalytic activity and good gas sensing properties.

One polyol synthesis of particular interest is that of 2D hexagonal Mn_2O_3 and Mn_3O_4 nanoplates reported by Liu *et al.*[71] In this synthesis, manganese acetate was used as the precursor in a mixture of EG and PEG. When PEG was not used, disk-shaped nanoplates were obtained over hexagonal ones. Through Fourier transform infrared (FTIR) analysis, the authors observed the gradual replacement of the acetate ligand for EG, thus yielding 2D hexagonal Mn-alkoxide nanoplates, as shown in Fig. 3a. Upon calcination of the Mn-alkoxide nanoplates at 500 °C for 2 h, there was complete conversion into Mn_2O_3 nanoplates as shown in Fig. 3b. Nanoplates of Mn_3O_4 were also obtained by submersion of the alkoxide nanoplates in deionized water for 12 h. This synthesis is particularly noteworthy due to the direct observation of a stable Mn-alkoxide product from a coordinating polyol, and then conversion into the phase-pure oxide. Furthermore, this study demonstrates the ability of polyols also to act as 2D shape directing agents.

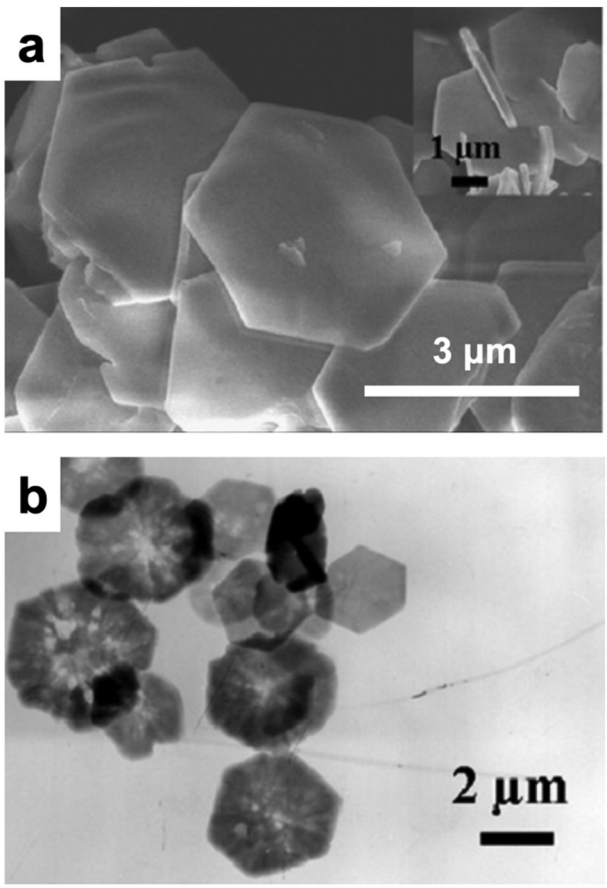

Fig. 3 (a) SEM image of manganese alkoxide nanoplates with inset showing a vertical standing nanoplate. (b) TEM image of Mn_2O_3 nanoplates obtained *via* calcination of the Mn alkoxide nanoplates. Reprinted from ref. 71. Copyright 2010, with permission from Elsevier.

In the synthesis of $CuFe_2O_4$ nanosheets by a polyol route, reported by the Zhen group,[69] the reaction pathway they propose is very similar to that of the Mn_2O_3 nanoplates synthesized by Liu, *et al.*, where there is observation of a 2D hybrid organic–inorganic intermediate.[71] The researchers utilized iron(III) chloride and copper(II) acetate as the starting precursors in EG media. Upon heating at 150 °C for 1 h, they obtained CuFe-glycolate nanosheets, as confirmed by XRD and FTIR analysis. The nanosheets were then calcinated at 350 °C for 3 h, which yielded $CuFe_2O_4/Fe_2O_3$. By SEM and TEM analysis, the authors observed that the $CuFe_2O_4/Fe_2O_3$ phase had a mesoporous nanosheet morphology comprised of smaller nanoparticles of the two phases formed by the decomposition of the glycolate precursor upon calcination. These porous $CuFe_2O_4/Fe_2O_3$ nanoplates were electrochemically studied and showed high charge capacity, as well as good cycle stability, making them potential candidates for next generation Li-ion batteries.

This polyol coordinating and shape-directing effect is present in almost all 2D oxide nanoplate syntheses. The coordinating ability of the polyols allows for the kinetically limited and highly anisotropic growth of these 2D oxide nanoplates. In the case of ZnO nanoplates,[70] the researchers utilized a polyol synthesis in which the components were zinc nitrate and hexamine in a solvent mixture of 30 : 10 DEG : H_2O. Hexamine is utilized as an ammonia source upon hydrolysis in solution and further dissociates into NH_4OH, where the hydroxide is the oxygen source. The product obtained was hexagonal ZnO nanoplates that, upon further TEM analysis, consisted of aggregated rod-shaped nanoparticles. When the researchers varied the precursors, amines, or solvents, they could not obtain these nanoplates. In this study, they proposed at a ratio of 30 : 10 DEG : H_2O, there is the coordination of the Zn(II) ions with DEG that leads to kinetic control of the nanorods while simultaneously forming nanoplates *via* the shape directing effect of the polyol, DEG.

Another important material that has been synthesized as 2D nanoplates by a polyol process is the quinary phase $LiNi_{1/3}Mn_{1/3}Co_{1/3}O_3$, or NCM, which is relevant as a cathode material for Li ion batteries.[74] For this polyol synthesis, the researchers used nitrates of lithium, nickel, and cobalt, along with manganese acetate, and heated them in EG at 85 °C for 8 h. The product subsequently underwent calcination at 800–900 °C for 8–16 h in order to obtain the NCM nanoplates as shown in the TEM image of Fig. 4. From HRTEM analysis, shown in the inset of Fig. 4, the authors conclude that the basal nanoplate planes are comprised of (001) planes and the edges are (010) planes. They propose that EG plays a critical

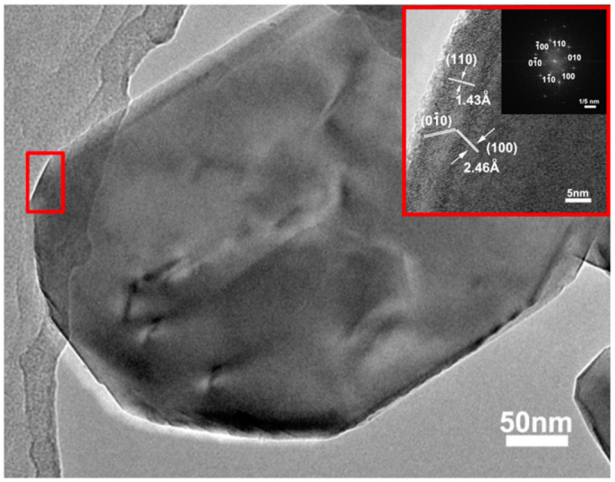

Fig. 4 $LiNi_{1/3}Mn_{1/3}Co_{1/3}O_3$ nanoplates synthesized in EG media. Adapted with permission from ref. 74. Copyright 2005 American Chemical Society.

role as a chelating agent for the metal ions, and together with its high viscosity, allows for a plate-directing effect and yields 2D NCM nanoplates. From XRD and SEM analysis, it is concluded that the nanoplates consist of highly ordered, hexagonal layers that form the nanoplate structure, enabled by the polyol shape-directing effect.

In a study carried out by the Yin group,[75] polyols were used in a post-processing technique to convert $Co(OH)_2$ into porous cobalt oxide hexagonal nanoplates with controllable oxygen vacancies, which were studied for their oxygen evolution reaction (OER) activity. The $Co(OH)_2$ nanoplates were synthesized by a previously established non-polyol solution method,[76] and were then injected into a solution of hot DEG at 220 °C and heated from 1–4 h with varying amounts of polyacrylic acid as a protecting agent. The authors observed the conversion of the $Co(OH)_2$ nanoplates into porous CoO_x nanoplates with different amounts of oxygen vacancies, as confirmed by XPS analysis, depending on the time and polyacrylic acid concentration. The oxygen vacancies of the nanoplates increase with reaction time in the DEG solution, indicating the solvent's reducing ability on the $Co(OH)_2$ precursor nanoplates. These CoO_x nanoplates with variable oxygen vacancies displayed remarkable performance for OER, with the most vacancies leading to the lowest achieved overpotential at 306 mV, making it one of the leading cobalt-based OER catalysts.

Other oxide materials that have been synthesized with 2D nanoplate morphology in an effort to make more efficient Li-ion battery materials are $LiFePO_4$ and $LiMnPO_4$.[72,73] In the synthesis of $LiFePO_4$ nanoplates, the authors utilized tetraethylene glycol (TEG) as the solvent, and upon heating the iron, lithium, and phosphate precursors at 335 °C for 12 h, they were able to obtain $LiFePO_4$ with 2D nanoplate morphology. The 2D morphology is attributed to the shape-directing effect of TEG and its ability to hydrogen bond to the nanoplate surface during growth. For the polyol synthesis of $LiMnPO_4$, the researchers were able to obtain nanoplatelets with thicknesses of ~20 nm by heating manganese, lithium, and phosphate precursors in DEG at 160 °C for 3 h. Both studies demonstrate the ability of polyol media to direct the 2D growth of different inorganic phosphate nanoplates. The $LiFePO_4$ and $LiMnPO_4$ nanoplates both showed good electrochemical properties, with high discharge capacities, making them potential Li-ion battery materials.

The 2D-directed growth of these oxide materials is largely dependent on the tendency of EG and other polyols to chelate to metal ions, which slows the reaction kinetics, and results in plate-like morphologies. In the case of NCM nanoplates, the EG molecules preferentially bind to the (001) facet, which slows the growth in that direction and leads to (010) facet to be exposed in a plate-like morphology.[74] The chelating effect, in addition to the higher viscosity of polyols which leads to diffusion-limited growth, ultimately results in these 2D oxide nanomaterials.

4. Chalcogenides

A rapidly growing class of 2D nanocrystals that have been synthesized *via* the polyol process are metal chalcogenides. Many chalcogenides are materials of interest in the fields of thermoelectrics,[77,78] optoelectronics,[79,80] and photocatalysis.[29] For example, the transition metal dichalcogenides (TMDs) possess strong light–matter interactions[81] and tetradymites (Bi_2Se_3, Bi_2Te_3, and Sb_2Te_3) contain topological insulating states from strong spin–orbit coupling,[82] which allow for remarkable optoelectronic and thermoelectric properties, respectively. These interesting physical properties enable a wide range of applications for 2D chalcogenide nanomaterials, which have been realized by polyol synthetic methods. The chalcogenide nanomaterials that have been synthesized with 2D morphology *via* a polyol process are outlined in Table 3.

One of the leading materials for optoelectronic and photocatalytic devices is CdS.[83–86] In a study by Wang *et al.*, the group was able to demonstrate effective shape control of the CdS nanocrystals depending on the injection rate of Cd^{2+} precursor into the reaction vessel containing excess sulfide precursor in tetraethylene glycol (TEG) medium.[87] A schematic of the nanocrystal growth is shown in Fig. 5a. The CdS nanocrystals that were obtained crystallized in the wurtzite structure type, where the surface energy of {0001} and {1011} facets dictate the nanocrystal growth in this synthesis. As detailed in Fig. 5b, when Cd^{2+} is injected into the solution in a single shot, the CdS monomers grow along the {1011} facets, creating a nanocone morphology. When the Cd^{2+} is injected more slowly (5 mmol h^{-1}), the CdS monomers react equally with the {1011} and {0001} facets, leading to a nanofrustrum morphology (shown in Fig. 5b). When the injection rate is further slowed (0.5 mmol h^{-1}), the concentration of the CdS monomer in solution is decreased, and preferentially reacts with the {1011} facet, leading to nanoplate morphology as shown in the TEM image of Fig. 5c. The PXRD patterns of the various mor-

Table 3 Chalcogenide nanomaterials synthesized with 2D morphology *via* a polyol process

Material	Morphology	Structure	Ref.
CdS	Nanoplates	Hexagonal (wurtzite)	87
CoS/CdS	Nanoplates	Hexagonal/hexagonal (wurtzite)	88
MoS_2/MWNTs	Nanoflowers	Hexagonal (2H phase)/MWNT	91
Cu_2Se	Nanoplates	Cubic (fluorite)	92
CuSe	Nanoplates	Hexagonal	93
CuS	Nanoplates	Hexagonal	94
In_2S_3	Nanoplatelets	Tetragonal	95
SnS	Nanoribbons	Orthorhombic	99
Bi_2Te_3	Nanoplates	Rhombohedral (tetradymite)	103, 106–110 and 112
Bi_2Se_3/Bi_2Te_3	Multishell nanoplates	Rhombohedral/rhombohedral (tetradymite)	117
$PbSe/Bi_2Se_3$	Vertical heterojunction nanoplates	Cubic (rock salt)/rhombohedral (tetradymite)	118
MoS_2	Nanosheets	Hexagonal (2H phase)	89 and 90
$Bi_{2-x}Sb_xTe_3$	Nanoplates	Rhombohedral (tetradymite)	108 and 112
Sb_2Te_3	Nanoplates	Rhombohedral (tetradymite)	101–105, 108 and 112
Bi_2Se_3	Nanoplates	Rhombohedral (tetradymite)	100, 106, 108 and 112
Sb_2Te_3/Bi_2Te_3	Core–shell nanoplates	Rhombohedral/rhombohedral (tetradymite)	115, 116 and 119
$Bi_2Se_{3-x}Te_x$	Nanoplates	Rhombohedral (tetradymite)	111–113 and 120

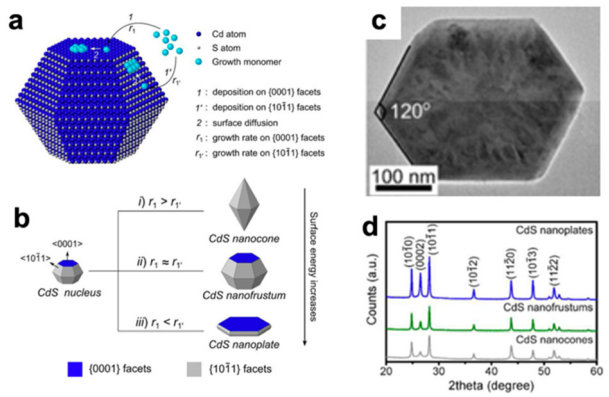

Fig. 5 (a) Schematic for the growth process of CdS nanostructures. (b) Formation of a CdS nanocone, a CdS nanofrustum, and a CdS nanoplate, obtained by different reaction rates. (c) TEM image of CdS nanoplate. (d) PXRD of various CdS nanostructures. Adapted with permission from ref. 87. Copyright 2015 American Chemical Society.

phologies obtained are shown in Fig. 5d, where there was an observed intensity change depending on the different nanocrystal morphology, and preferred orientation along the (0002) plane can be observed in the nanoplates pattern. Furthermore, another group was able to create heterostructures of CdS nanoparticles decorated on 2D CoS hexagonal nanoplates.[88] The CoS nanoplates were synthesized *via* a multi-step non-polyol method, and CdS nanoparticles were subsequently grown onto the CoS surface *via* a polyol process. The final product they obtained was well-defined hexagonal nanoplates of CdS decorated CoS, which was further confirmed by XPS analysis. These two studies demonstrate how polyols enable the nucleation and growth of CdS nanostructures, and how 2D morphology may be kinetically controlled in the syntheses.

The TMDs, such as MoS_2, are being heavily investigated in the field of catalysis due to their high activity for the hydrogen evolution reaction (HER).[29] Several groups have reported on the synthesis of 2D MoS_2 nanomaterials *via* the polyol method, with nanoflower and nanosheet morphologies.[89,90] These groups were motivated to prepare 2D MoS_2 nanomaterials for HER catalysis, as well as creating high-defect structures for humidity sensing. Leng *et al.* report a three-step growth mechanism to obtain MoS_2 nanosheets in polyol media.[89] First, using a heptamolybdate salt and thiourea in a mixture of water and a polyol, MoS_2 nucleates into nanocrystal seeds. Next, the MoS_2 seeds continuously grow while also forming clusters. Finally, 2D MoS_2 nanoflakes grow from the clusters, resulting in a nanoflower morphology. The researchers studied the effect of various polyol/water mixtures and found that PEG and water produced the best 2D nanoflower morphology, whereas the other polyols produced smaller nanoflakes with more bulk-like morphology. They propose the difference in morphology is due to the higher reducing power of the shorter chain polyols, which creates more defective MoS_2.

In a report on MoS_2 nanosheets by Wang *et al.*, a mixture of EG or DEG and water was used as the solvent.[90] The different polyols served as the reducing agent of the molybdenum salt precursor, along with sulfur powder, in a proposed three-step mechanism. The reaction progresses by first nucleation and growth of MoS_3 nanoparticles, which get further reduced to form MoS_2 nanoflakes, and finally upon aggregation form nanosheets with an average length of 150 nm and varying thicknesses. The nanosheets were confirmed to consist of aggregated nanosheets by HRTEM and SAED analysis. The researchers attribute the formation of nanosheets from smaller nanoflakes to the reduction in total energy of the system. Varying the polyol from EG to DEG, allowed the researchers to control the lateral size of the nanosheets due to the higher viscosity and additional hydrogen bond accepting property.

Zhang *et al.* used a polyol method to grow highly crystalline 2D MoS_2 nanostructures epitaxially on multi-walled nanocarbon tubes (MWNTs) which were investigated as an anode material for Li-ion batteries.[91] The MoS_2 hybrid was

synthesized using a traditional coating synthesis in which the molybdenum and sulfur precursors were added to a suspension of the MWNTs in DEG and grown epitaxially. The product they obtained was nanoflowers of the MoS_2 nanosheets grown onto the MWNTs, which was enabled by the reduction of precursors in DEG media and their subsequent heterostructure growth. By HTREM analysis, the researchers found that the interlayer spacing had increased in the MoS_2 from the lattice mismatch of the heterostructure, which enables higher Li ion storage capacity. It was concluded that these heterostructures had much higher charge capacity than MoS_2 alone, making them promising materials for Li ion batteries.

Copper chalcogenide 2D nanomaterials, such as Cu_2Se,[92] CuSe[93] and CuS[94] nanoplates, have been successfully synthesized *via* the polyol method and reported in the literature. Zhu *et al.* synthesized 2D nanoplates of Cu_2Se *via* a microwave-assisted polyol method, which were then studied as electronically conductive thin films.[92] The researchers of this study showed that Cu_2Se nanoplates could be synthesized *via* the microwave-assisted polyol reaction due to the good thermal stability and fast reduction kinetics in polyol solvent but were unable to achieve well-defined 2D morphologies *via* solvothermal or solution routes. Another copper selenide 2D nanomaterial, CuSe, was synthesized by Liu *et al. via* the polyol method.[93] This group used triethylene glycol (TEG) in the presence of thioglycolic acid (TGA) and monoethanolamine (MEA) to yield the nanoplates, whose morphology is primarily dictated by the lamellar hexagonal crystal structure. The hexagonal nanoplate morphology was confirmed by TEM, and the crystal structure was confirmed by SAED and PXRD analyses. CuS nanoplates have also been synthesized by Fu *et al.* and shown promise for photocatalytic devices.[94] In this synthesis, the researchers could kinetically control product morphology by changing the sulfur precursor. Varying the precursor from elemental sulfur to sulfide salts led to an increased rate of sulfide release and, thus, more ill-defined nanoplates, which grew into nanoflowers. In using elemental sulfur, the polyol media must first reduce the precursor, which leads to a lower release rate and yields well defined hexagonal nanoplates.

In another polyol synthesis, the Mukherjee group was able to successfully synthesize 2D nanoplatelets of In_2S_3 with a thickness of ~7 nm.[95] The researchers carried out photoconductance measurements on these ultrathin In_2S_3 nanoplatelets, which showed an improvement of two orders of magnitude from the dark conductivity, making them viable materials for solar cell applications. This synthesis utilizes $InCl_3$ and thiourea as the precursors in ethylene glycol and is assisted by 1-thioglycerol. After heating the reaction solution at 140 °C for 1 h, it was cooled to room temperature, and the nanoplatelets were recovered by centrifugation. From SEM and TEM analysis, the authors confirm that the nanoplatelets have round morphology with ill-defined edges, and a uniform thickness of ~7 nm. Using SAED analysis, the nanoplatelets are elucidated to be highly crystalline and correspond to the tetragonal In_2S_3 structure type. Through systematic investigations of the reaction product without 1-thioglycerol as an additive, the researchers confirmed that the uniformity in the lateral and thickness distribution is larger. With these studies, they are able to propose that the 1-thioglycerol acts as binding agent on the sulfur residues of the nanoplatelet and serve as a shape-directing component.

One material of interest as a potential photodetector,[96] as well as thermoelectric,[97,98] is SnS and its alloys $SnS_{1-x}Se_x$. Nanoribbons of SnS that were synthesized in ethylene glycol media have been reported in the literature by Chao *et al.*[99] The SnS nanoribbons were 10–20 nm in thickness, with widths of 200–500 nm and lengths of several microns. Upon HRTEM analysis, the researchers observed that the nanoribbons were polycrystalline and belonged to the orthorhombic SnS phase. The researchers also carried out time dependent studies of the reaction dynamics and observed that there are only micron sized spheres in the initial stage of the reaction, which develop into nanoribbons after 1.5 h and finally are well defined polycrystalline nanoribbons after 2.5 h. In this study, the morphology is largely dictated by the crystal structure of the material, which was synthesized in the presence of polyol media. These SnS nanoribbons demonstrated good photocurrent density, which expands the field of flexible photodetectors.

The leading materials for room-temperature thermoelectric devices are the tetradymite structures of Bi_2Te_3, Bi_2Se_3, and Sb_2Te_3, which have been previously synthesized as hexagonal nanoplates *via* polyol processes.[100–108] Hexagonal nanoplates of Bi_2Se_3 were synthesized by Lin *et al.* using EG in the presence of PVP which serves as a capping agent.[100] The nanoplates were found to be ultrathin, with a thickness of ~6 nm, by AFM analysis. The authors used these 2D nanoplates to create flexible electronic films that are highly IR transparent. The Tanemura group has reported on the facile synthesis of single-crystalline Sb_2Te_3 with good thermoelectric figure of merit.[102] The morphology of the Sb_2Te_3 nanoplates could be controlled by changing the surfactants in the synthesis, and was found that PVP yielded the best hexagonal 2D nanoplate morphology. In another study on the polyol synthesis of Sb_2Te_3 nanoplates, it was demonstrated that increasing the concentration of PVP in the reaction decreased the thickness of the nanoplates, due to higher surface coverage and kinetic control.[101] This led to enhanced thermoelectric properties in the thinner nanoplates. This advancement illustrates the applicability of polyols to give rise to desired materials properties.

Our group has reported on the synthesis and thermoelectric properties of 2D hexagonal Bi_2Te_3 and Sb_2Te_3 nanoplates and their composites, in which the properties are systematically changed by adjusting the nanoplate composition.[103] We demonstrated that different polyols enable the synthesis of the two types of Bi_2Te_3 and Sb_2Te_3 nanoplates as shown in Fig. 6a and b, respectively. The Bi_2Te_3 nanoplates are synthesized at a lower reaction temperature (185 °C) in EG, whereas the Sb_2Te_3 nanoplates require higher reaction temperatures (210 °C), and the synthesis is carried out in DEG. Through the synthesis and compositing of these nanoplates, we were able to achieve one of the highest thermoelectric figures of merit (zT) for this

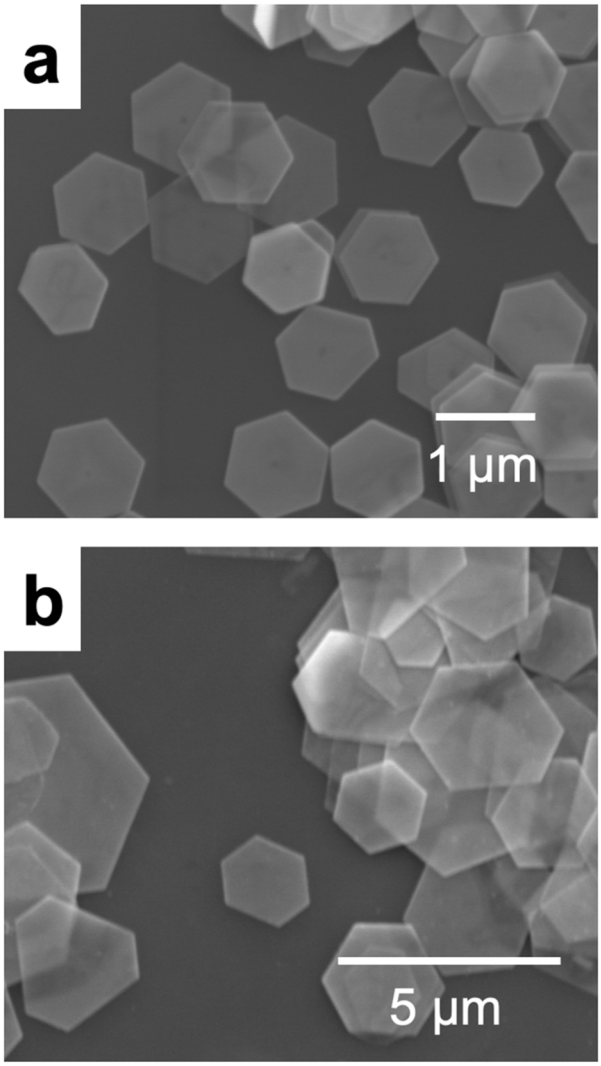

Fig. 6 SEM images of (a) Bi_2Te_3 nanoplates and (b) Sb_2Te_3 nanoplates. Adapted from ref. 103 (open access).

system, with a maximum zT = 1.26. Dun *et al.* reports the synthesis of Bi_2Te_3 nanoplates with a single nanopore in the center.[109] This group was able to create a single nanopore in the center of Bi_2Te_3 nanoplates with a temperature controlled post-processing technique in EG. This technique enabled the rediffusion of the Bi and Te atoms, subsequently leaving behind a hole in the center of the nanoplate. Our group has also synthesized Bi_2Te_3 nanoplates with a single nanopore in the center *via* the polyol technique, demonstrating ultralow lattice thermal conductivity in this material.[110]

Several groups have investigated alloys of these tetradymite nanoplates and have seen improvements in the thermoelectric properties.[111–113] Our group has reported on doping studies of Sb into Bi_2Se_3 nanoplates where an increase in carrier mobility of the material is observed.[114] Several different chalcogenide inks, with various compositions, were created from colloidally synthesized 2D nanocrystals by Zeng *et al.*[112] Their work provides insight into the polyol synthesis of tetradymite nanoplates, as they demonstrate successful synthesis of Bi_2Te_3, Bi_2Se_3, Sb_2Te_3, as well as their alloys. The researchers find that different reaction temperatures are optimal for various nanoplate compositions, and they achieve this by creating so-called "solvent engineered colloidal synthesis (SCS)" methods or by using mixed polyol solvents. With the SCS method, they could create pure phase nanoplates of various alloyed compositions.

Heterostructures of Bi_2Te_3 and Sb_2Te_3 materials has been greatly explored by additional groups.[115–118] Core shell Bi_2Te_3/Sb_2Te_3,[115,119] as well as multishell Bi_2Te_3/Bi_2Se_3,[117] nanoplates that were obtained *via* polyol routes have been reported in the literature. Additionally, there have been Bi_2Te_3/Sb_2Te_3 lateral heterojunction nanoplates reported that were also synthesized *via* a polyol method.[116] In each of these syntheses, the core nanoplate, which is Bi_2Te_3, is first grown in EG and then the shell/lateral material is epitaxially grown onto the core using metal salt precursors. These heterostructured nanoplates often show high crystallinity and sharp interfaces by HRTEM and EDX analysis. Our group has reported on synthesizing Bi_2Te_3/Sb_2Te_3 core–shell nanoplates using a polyol method.[119] We synthesized the core–shell nanoplates and subsequently consolidated the nanoplates into a densified material, on which the thermoelectric properties were studied. 2D heterojunction nanoplates of Bi_2Te_2Se/Bi_2Te_3 were previously synthesized by Bauer *et al.*, as well as doped Bi_2Te_2Se.[120] This group systematically varied the Te to Se ratio, to control the final composition of the heterostructured nanoplates.

Additionally, 2D PbSe/Bi_2Se_3 heterostructures have been studied by Lin *et al.*, which were synthesized *via* the polyol route.[118] First the Bi_2Se_3 nanoplates were synthesized, and then the PbSe was epitaxially grown on top by slow injection of the precursors into the EG media, yielding a vertical heterostructured nanoplate, as shown in the TEM image of Fig. 7a. A clear moiré pattern can be seen in the HRTEM image of the heterostructure shown in Fig. 7b, which indicates a lattice mismatch. The PbSe, which crystallizes in the rock-salt structure type, adopts a 2D morphology because the growth is templated by the Bi_2Se_3 nanoplate. This epitaxial growth can be deduced from the SAED pattern in Fig. 7c, which shows the rock-salt lattice diffraction from PbSe in addition to the hexagonal tetradymite diffraction pattern of Bi_2Se_3. Fig. 7d and e show the crystal structures of PbSe and Bi_2Se_3, respectively, indicating a small lattice mismatch. The heterostructure growth is enabled by the small lattice mismatch in the *c* crystallographic direction as shown in Fig. 7f. This is quite a unique and noteworthy synthesis because it exemplifies the versatility of polyol solvents to enable the growth of 2D heterostructure nanoplates with dissimilar structure types.

Despite the fact that many 2D chalcogenide materials are inherently layered materials, which enable 2D growth, polyols are able to further enhance the quality of the 2D morphology. When using polyols, in the place of other common solvents such as oleylamine or dodecanethiol, typically the crystal facets of these chalcogenide materials are much shaper and well defined. Specifically for the tetradymite materials (Bi_2Te_3, Bi_2Se_3, and Sb_2Te_3) and their alloys, ethylene glycol is almost

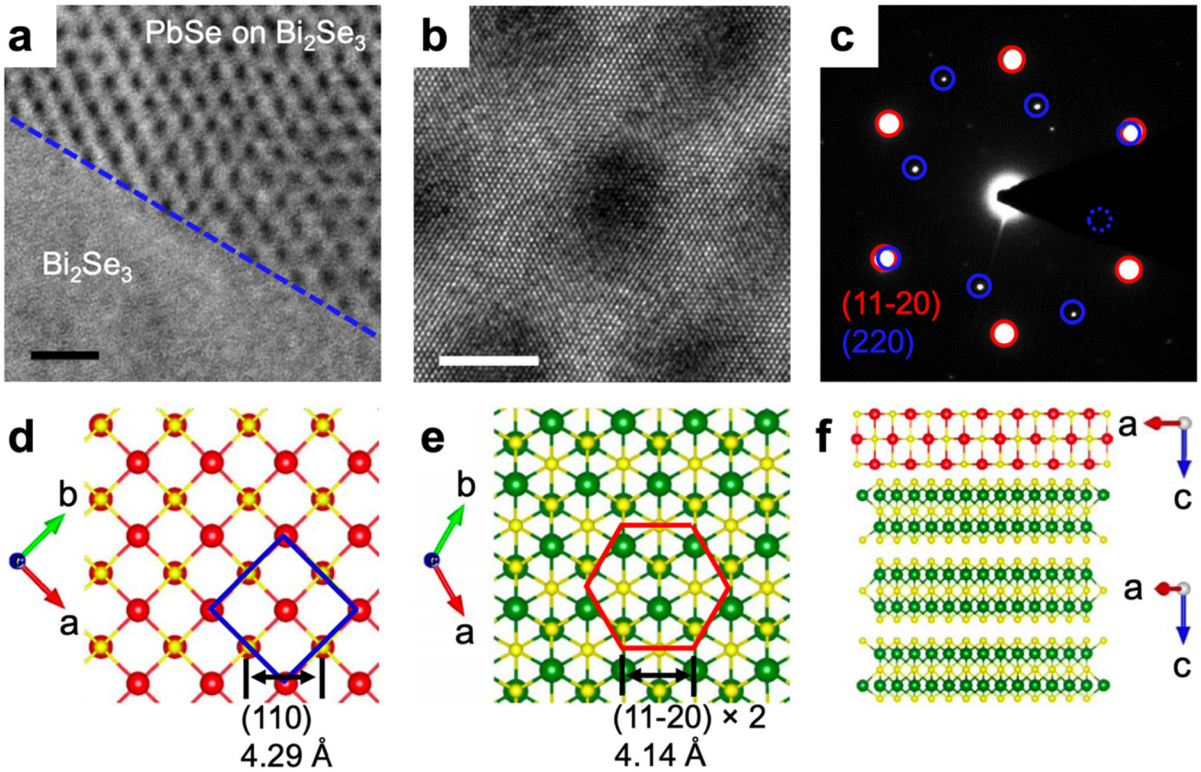

Fig. 7 (a) TEM image of a top view of the heterostructure. (b) A HRTEM of a PbSe/Bi_2Se_3 region showing a moiré pattern. (c) A SAED of the heterostructure. (d) The crystal lattice of PbSe. (e) The crystal lattice of Bi_2Se_3. (f) A schematic of the epitaxial growth of the heterostructure. Adapted from ref. 118 (open access).

exclusively used in the synthesis. Other studies using thiols as the solvent, such as ultrathin Bi_2Te_3 nanoplates reported by Son *et al.*,[17] display materials with ill-defined facets. This likely is due to the binding strength of sulfur *versus* oxygen, in the context of hard–soft acid–base (HSAB) theory, where sulfur is soft and interacts strongly with the soft chalcogenide ions, and oxygen is hard which has a weaker interaction. One may conclude that the weak interaction of the oxygen atoms of EG to these chalcogenide materials, mechanistically leads to kinetic control of these 2D structures.

5. Halides

The final class of materials that will be discussed in this review are the 2D halide nanostructures. Although there have been a significant number of reports on the solution synthesis of 2D halide nanostructures,[121–125] there are a very limited number of synthetic methods that utilize polyol media, as described in Table 4.[126–128] Typical polyol syntheses of 2D halide nanomaterials are surfactant-free, although they often utilize various salts as mineralizers for the selective crystallization of the desired phase. The ability to include additives in conjunction with the coordinating and shape directing effects of the polyol allow for the realization of high quality 2D halide nanocrystals.

Table 4 Halide nanomaterials synthesized with 2D morphology *via* a polyol process

Material	Morphology	Structure	Ref.
LaF_3	Nanoplates	Hexagonal	126
CeF_3	Nanoplates	Hexagonal	127
CuI	Nanosheets	Cubic (zinc blende)	128

The rare earth halide, LaF_3, was synthesized as 2D hexagonal nanoplates by a polyol process reported by Qin *et al.*[126] These LaF_3 nanoplates may find applications in optoelectronics or biological detection. The hexagonal nanoplates had a diameter of ~65 nm (Fig. 8a) and thickness of ~20 nm (Fig. 8c). Through electron diffraction studies, the authors confirmed that the basal planes consisted of {0001} planes (Fig. 8b) and the edges were {10−10} planes (Fig. 8d) of the hexagonal LaF_3 structure type. In this study, the researchers utilized lanthanum(III) nitrate and NH_4F as the precursors with $NaNO_3$ as an additive in EG media and heated the solution at 180 °C for up to 48 h. Many synthetic parameters were systematically varied in order to deduce the mechanism of formation for these 2D hexagonal nanoplates.

Replacing the solvent from EG to DEG, water, methanol, or glycerol in this synthesis yielded different morphologies. There was no obvious change in the morphology when using DEG as

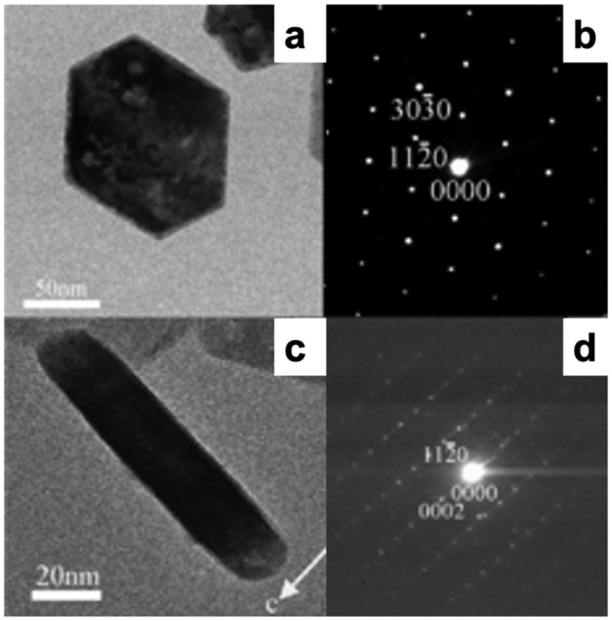

Fig. 8 (a) TEM of LaF_3 nanoplate lying flat and (b) corresponding SAED pattern. (c) TEM of LaF_3 nanoplate standing on side and (d) corresponding SAED pattern. Adapted with permission from ref. 126. Copyright 2009 American Chemical Society.

the solvent; however, when using water or methanol, small nanoparticles were obtained simultaneously with irregular nanoplates. When glycerol was used, the product resulted in only LaF_3 nanoplates, although they had irregular shapes and a broad size distribution. These studies demonstrate the ability of polyol solvents to kinetically limit the 2D anisotropic growth of LaF_3 nanomaterials.

Furthermore, Qin *et al.* varied the concentration of NH_4F and $NaNO_3$ in the solution synthesis of these LaF_3 nanoplates. When the concentration of NH_4F was too low, only small nanocrystals were obtained, and when the concentration was further increased, hexagonal nanoplates were the selected product. Interestingly, when $NaNO_3$ concentration was changed, the reaction progressed *via* different pathways. With no $NaNO_3$ nitrate as an additive, the hexagonal LaF_3 phase initially nucleated and grew into thick and irregular nanoplates, as confirmed by XRD and SEM analysis. However, when $NaNO_3$ was added to the reaction, the hexagonal LaF_3 phase formed first, then as the reaction progressed past 2 hours, was converted into another intermediate phase that could not be identified by XRD, finally converting back to the hexagonal LaF_3 phase after 24 h. After 24 h, the product obtained was well-defined hexagonal LaF_3 nanoplates with constant uniform thicknesses. These results indicate that sodium ion could adsorb onto the surface of specific crystal facets in the presence of a polyol, allowing for the selective growth of well-defined LaF_3 2D nanoplates.

Another rare-earth fluoride that has been synthesized with 2D nanoplate morphology by a polyol route is CeF_3 and Tb-doped CeF_3.[127] The authors of this study were able to selectively obtain hexagonal 2D nanoplates of CeF_3 and CeF_3:Tb^{3+} by reacting the precursors, cerium(III) nitrate, terbium(III) nitrate and NH_4F, in EG media, and systematically varying the NH_4F content. As in the case of hexagonal LaF_3 nanoplates,[126] the best morphology for the CeF_3 nanoplates is at higher NH_4F concentrations of 24 and 36 mmol compared to 6 mmol, which yielded only nanoparticles. This study did not use any salt additives, which can be used as a fine-tuning parameter in these reactions, and thus, the nanoplates they obtained grow both in diameter ranging from 65–210 nm and thickness ranging from 20–70 nm as NH_4F is increased. The overall 2D growth morphology is primarily governed by the anisotropic hexagonal crystal structure, which is the same as that of LaF_3, but also by the shape directing effects of the fluoride ions in the presence of polyol media. These nanoplates showed remarkable photoluminescence properties that could be tuned with the size of the nanoplates, due to the varying amount of surface defects.

The last example of 2D nanostructures synthesized by a solution polyol process is CuI nanosheets reported by the Ba group.[128] The electrical conductivity of these CuI nanosheets was shown to be greatly enhanced compared to the bulk counterpart, making it an attractive electronic material. The researchers employed PEG as the solvent with potassium iodide and copper(II) chloride as the precursors. The reaction included sodium dodecyl benzenesulfonate (SDBS) and $NaNO_3$ as additives. A solution of the precursors and SDBS was added dropwise to a $NaNO_3$ solution at room temperature, and the CuI nanoplates were precipitated. The effect of SDBS was investigated in conjunction with the PEG media and it was concluded that without SDBS present, there was poor nanosheet formation, and only at higher SDBS concentrations were well-defined nanosheets obtained. The nanosheets were 60–80 nm thick and had lateral dimensions of several microns. X-ray and electron diffraction studies confirm that the basal nanoplate facets consist of the (111) planes of the marshite structure type. From Raman and TEM analysis of the precursor solution, the researchers confirm that PEG acts as a complexing agent for Cu(I) ions and prevents the formation of CuI nanoparticles. Once the reaction is initiated by addition to the $NaNO_3$ solution, CuI nanoplates grow *via* adsorption of PEG onto the (111) facets and promote the 2D nanosheet growth. The synthetic studies carried out in this report highlight the synergy of polyols, ions, and surfactants to enable anisotropic growth through adsorption to specific crystal facets, allowing the formation of 2D CuI and potentially other transition metal halides.

Halide nanomaterials with 2D morphology are typically achieved by including additives and mineralizers, which are typically simple elemental or polyatomic ions, into the polyol mixture. The mineralizers serve to bind to crystal facets and promote dissolution and re-precipitation of the nanocrystals, leading to 2D growth. It is plausible that the lower polarity of polyols, compared to water, allows for the mineralizers to associate with the nanoplate surface instead of undergoing complete solvation by the solvent environment. These minera-

lizers work synergistically with the polyol to bind to nanoplate surfaces and promote the 2D growth.

6. Applications

There are a myriad of fields the 2D nanomaterials discussed in this review find practical applications in, ranging from Li-ion batteries to thermoelectricity. Many leading Li-ion cathode materials are layered oxides and phosphate materials, that have seen enhancements to electrochemical performance with 2D morphology.[74,129] Other oxide and chalcogenide 2D nanomaterials are particularly relevant for photocatalytic applications, such as organic contaminate degradation or H_2 evolution.[68,87] Metallic 2D nanomaterials are of interest for plasmonic applications, often serving as superior substrates for surface enhanced Raman spectroscopy (SERS).[53,63] Nanoplates of the layered tetradymite structure type show excellent thermoelectric performance due to low thermal conductivity and electronic carrier effects at the nanoplate interfaces.[100–103] In this section, we describe the relevant 2D nanomaterials for various applications that have been synthesized *via* a polyol process.

6.1. Li-ion batteries

A handful of oxide ($LiNi_{1/3}Mn_{1/3}Co_{1/3}O_3$ (NCM)) and phosphate ($LiFePO_4$ and $LiMnPO_4$) 2D nanomaterials are of interest as Li-ion batteries cathode materials, due to their high Li-ion conductivity, as well as high capacity. An important attribute to these cathode materials is high cycling stability, as well as high capacitance, which was obtained in 2D nanoplates of NCM synthesized *via* the polyol route.[74] The authors of this study grew the NCM nanoplates with active (010) planes exposed, which allowed for the high discharge capacity (207.6 mA h g^{-1}) and the best capacity retention among any NCM nanoplate materials (89.4%), as shown in Fig. 9.

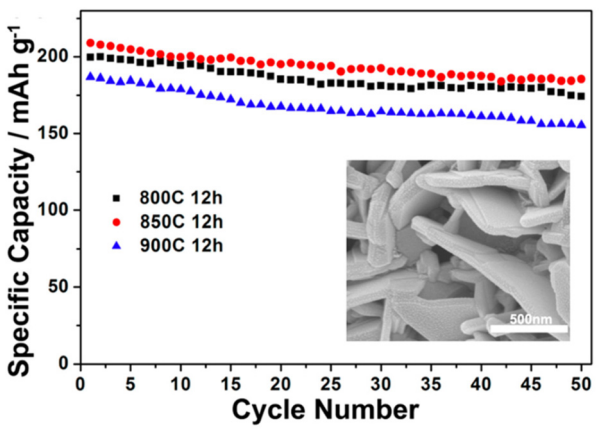

Fig. 9 Electrochemical performance of 2D $LiNi_{1/3}Mn_{1/3}Co_{1/3}O_3$ (NCM) nanoplates for samples sintered at various temperatures (800, 850, and 900 °C). Inset shows a SEM micrograph of typical NCM nanoplates. Adapted with permission from ref. 74. Copyright 2005 American Chemical Society.

Other promising Li-ion battery cathode materials are those of the olivine structure type ($LiFePO_4$). The three-dimensional crystal structure allows for excellent Li-ion conductivity and have been reported as 2D nanoplates synthesized *via* polyol media. Both the Fe and Mn analogs of the olivine structure type have been grown as 2D nanoplates this way and show high first discharge capacities of 166 and 129 mA h g^{-1}, respectively.[72,73] Furthermore these 2D nanomaterials exhibit robust capacity retention. These studies establish 2D oxide nanomaterials as promising candidates for highly efficient Li-ion battery cathode materials.

6.2. Photocatalysis

Many oxide and chalcogenide 2D nanomaterials are promising candidates for photocatalysis due to their large surface area and strong light–matter interactions.[130,131] The hematite structure type (α-Fe_2O_3) is a very well-known photocatalyst for degradation of organic contaminates.[132] α-Fe_2O_3 nanoplates that were synthesized *via* a polyol route by Hao *et al.*, were investigated for their photocatalytic degradation of Rhodamine B (RhB), and their activity in the presence of H_2O_2 is shown in Fig. 10a.[68] The authors refer to the nanoplates as samples A, B, and C which denote different dimensions of the nanoplates ranging from 30 to 40 nm in thickness and 180 to 740 nm laterally. The nanoplate samples display enhanced photocatalytic degradation of RhB compared to the blank (only RhB and H_2O_2), where the nanoplates with the largest lateral dimension are the most active (sample C).

Another promising photocatalytic material with 2D morphology is CdS.[85] Various morphologies of polyol-synthesized CdS nanostructures that were synthesized *via* kinetic control were studied for their photocatalytic H_2 production in aqueous solution.[87] CdS nanocones, nanofrustums, and nanoplates were all investigated and show high activity for photocatalytic H_2 production, however it was observed that the nanoplate morphology was the most active, shown in Fig. 10b. The photocatalytic H_2 production for the CdS nanoplates was 2.3 and 1.6 times higher than nanocones and nanofrustums, respectively. The average H_2 production was highest for the nanoplate morphology as seen in Fig. 10c, and the specific activity was confirmed to be the greatest for this morphology, as shown in the inset of Fig. 10c. These results corroborate the superiority of 2D nanomaterials for photocatalytic applications, compared to other nanocrystal morphologies.

6.3. Plasmonics

Many leading plasmonic materials are noble metals such as Au, Ag, and Pd, due to the highly delocalized sea of electrons.[133,134] These plasmonic properties are greatly enhanced with 2D morphologies and can be further tuned by creating different lateral sizes of nanoplates. These metallic 2D nanomaterials find applications in surface enhanced Raman spectroscopy (SERS), which enables detection of molecular species at very low concentrations. Both Au and Pd nanoplates synthesized *via* a polyol route find applications in SERS, which have enabled the detection of low concentrations of rhoda-

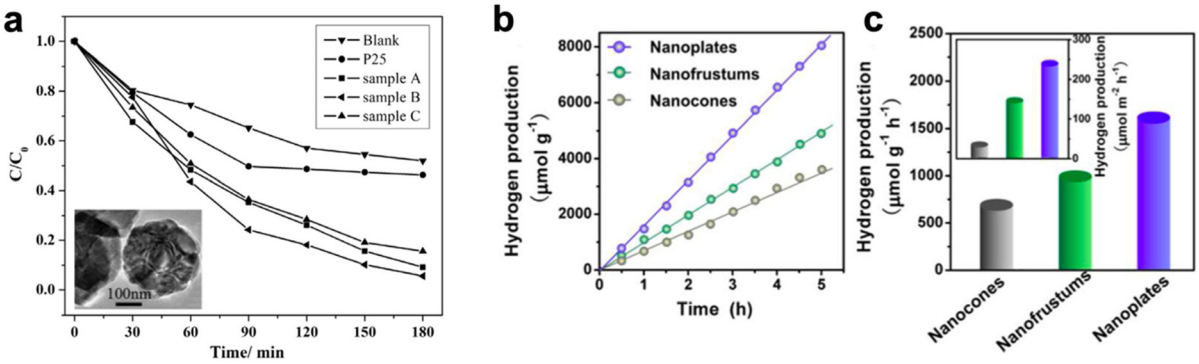

Fig. 10 (a) Photocatalytic degradation of RhB by hematite nanoplates. The legend denotes various samples of nanoplates with different thickness and lateral dimensions and the blank (only RhB and H_2O_2). Inset shows a TEM image of typical hematite nanoplates. Adapted with permission from ref. 68. Copyright 2015 Elsevier. (b) Photocatalytic H_2 production over time and (c) average photocatalytic H_2 production by CdS nanostructures in aqueous media. Adapted with permission from ref. 87. Copyright 2015 American Chemical Society.

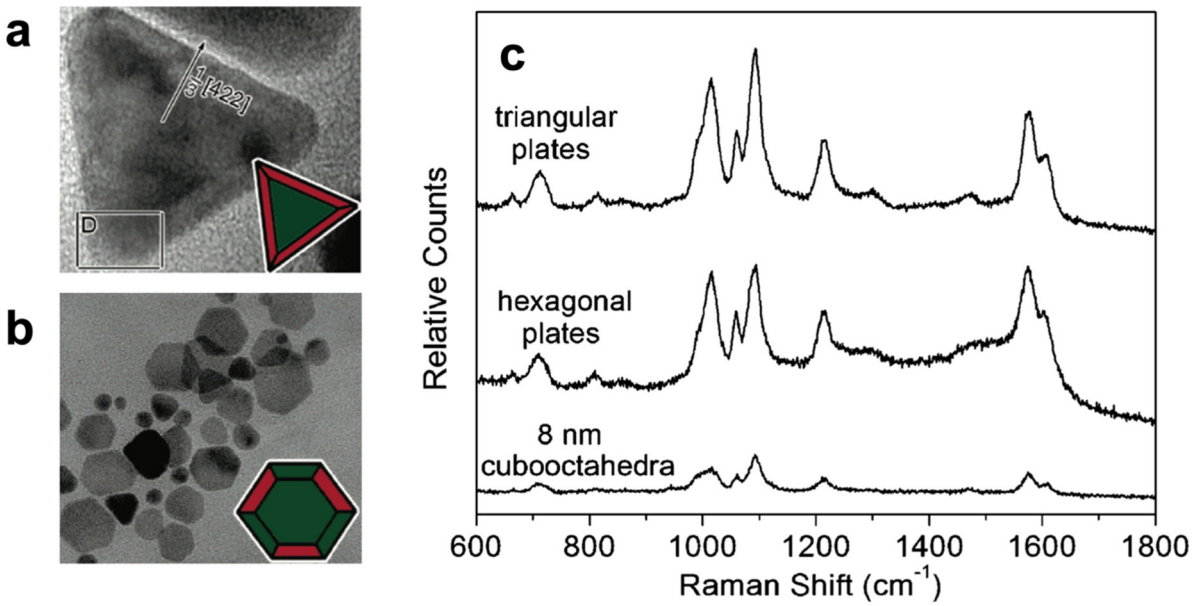

Fig. 11 TEM image of (a) triangular and (b) hexagonal Pd nanoplates synthesized *via* a polyol route. (c) Surface enhanced Raman spectra (SERS) of 2-mercaptopyridine adsorbed onto various Pd nanostructures. Adapted with permission from ref. 63. Copyright 2005 American Chemical Society.

mine 6G and 4-mercaptopyridine, respectively.[53,63] The SERS spectra of 4-mercaptopyridine adsorbed onto Pd nanomaterials is shown in Fig. 11. There is a 4.3- and 3.4-times enhancement observed for the molecule adsorbed onto triangular and hexagonal Pd nanoplates, respectively, compared to Pd nanoparticles. These findings set the precedent for metallic 2D nanomaterials as promising candidates for the next generation of plasmonic materials.

6.4. Thermoelectricity

The current state-of-the-art room-temperature thermoelectrics are those of the tetradymite structure type (Bi_2Se_3, Bi_2Te_3, and Sb_2Te_3, and their alloys).[82,135] The extraordinary thermoelectric properties of these materials are due to the high crystal high symmetry, leading to high electronic band degeneracy, as well as inherently low lattice thermal conductivity. High band degeneracy ultimately leads to large Seebeck coefficients, caused by high density of states near the Fermi level. The layered tetradymite structure also contributes to low lattice thermal conductivity, which can be lowered even further through enhanced phonon scattering due to the nanoplate morphology. There are many reports of polyol-synthesized tetradymite nanoplates that show good thermoelectric performance. In a study carried out by our own group, we observed an enhanced thermoelectric figure of merit (zT) for nanoplate composites of Bi_2Te_3 and Sb_2Te_3 (0–25% Bi_2Te_3 into Sb_2Te_3) that were synthesized *via* a polyol route, as shown in Fig. 12.[103] Thermoelectric property measurements perpendicular to the

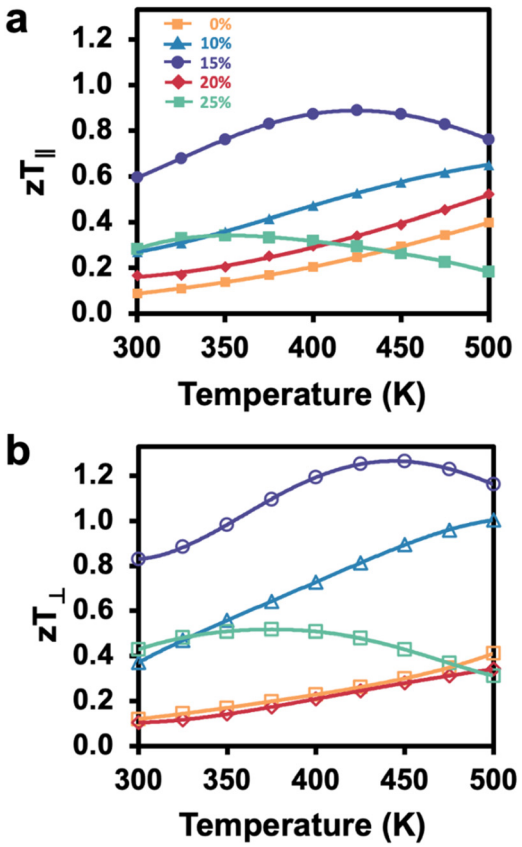

Fig. 12 Thermoelectric figure of merit (zT) for composites of Bi_2Te_3 and Sb_2Te_3 nanoplates (0–25% Bi_2Te_3 into Sb_2Te_3) that were synthesized *via* a polyol route, measured (a) parallel and (b) perpendicular to nanoplate basal planes. Adapted from ref. 103 (open access).

nanoplate basal planes show superior thermoelectric performance than parallel to nanoplate basal planes, as shown in Fig. 12a and b, respectively. The enhanced thermoelectric properties are due to the low thermal conductivity attributed to significant phonon scattering at ultrathin 2D nanocrystal domains. In this study, a maximum $zT \sim 1.26$ was obtained, which is one of the highest reported for this system. These findings, and others in the field, corroborate the benefit of implementation of 2D nanomaterials in thermoelectric applications.

7. Conclusions and outlook

This review has presented the various material classes, including metals, oxides, chalcogenides, and halides, that have been synthesized as 2D nanomaterials using a polyol process. Many of these syntheses utilize metal salt precursors, which readily dissolve in polyol media, with surfactants or additives that act as 2D growth directing agents. Typically, in the synthesis of 2D metal nanomaterials like gold and silver, surfactants such as polyvinylpyrrolidone (PVP), bind to specific crystallographic planes to kinetically control 2D growth. We find that in the case of many oxides, the polyol solvent itself acts as a binding agent which serves to control 2D growth of the material. Additionally, we review how polyols have been used extensively to synthesize many 2D chalcogenide nanoplates, including the tetradymites (Bi_2Se_3, Bi_2Te_3, and Sb_2Te_3), transition metal dichalcogenides (TMDs) like MoS_2, wurtzite CdS, and even heterostructures. Finally, we discuss a number of examples where 2D halide nanomaterials have been synthesized in polyol media. The versatility of reagent solubility, boiling points, and binding affinity allow for the design of synthetic procedures that enable the growth of high-quality and well-defined 2D nanomaterials. We believe that the polyol synthetic process is extremely versatile and has enabled the realization of many 2D nanomaterials, opening doors for further synthetic exploration. The polyol syntheses may be extended to other systems, which are but not limited to, noble metals, other TMDs ($MoSe_2$, WS_2, WSe_2, *etc.*), oxides, layered double hydroxides (LDHs), halides, heterostructures, and others, to form 2D nanocrystals. In conclusion, the various reports on 2D nanocrystal synthesis *via* polyol processes have shown high fidelity and control, successfully enabling the realization of an array of 2D nanomaterials. The field continues to expand and holds much promise for the next generation of high quality 2D nanocrystals.

Data availability

Original literature is referenced and primary data can be retrieved from those sources.

Conflicts of interest

There are no conflicts to declare.

Acknowledgements

This work was supported by the National Science Foundation, DMR-2001156, and DMR-2335203.

References

1 K. S. Novoselov, A. K. Geim, S. V. Morozov, D. Jiang, Y. Zhang, S. V. Dubonos, I. V. Grigorieva and A. A. Firsov, Electric Field Effect in Atomically Thin Carbon Films, *Science*, 2016, **306**, 666–669.
2 H. Cai, Y. Gu, Y. C. Lin, Y. Yu, D. B. Geohegan and K. Xiao, Synthesis and emerging properties of 2D layered III-VI metal chalcogenides, *Appl. Phys. Rev.*, 2019, **6**, 1–30.
3 Y. Min, E. Im, G. T. Hwang, J. W. Kim, C. W. Ahn, J. J. Choi, B. D. Hahn, J. H. Choi, W. H. Yoon, D. S. Park, D. C. Hyun and G. D. Moon, Heterostructures in Two-Dimensional Colloidal Metal Chalcogenides: Synthetic

Fundamentals and Applications, *Nano Res.*, 2019, **12**, 1750–1769.
4 Z. Cheng, J. Sun, B. Zhang, Z. Lu, F. Ma, G. Zhang and Q. Xue, Strain Effects of Vertical Separation and Horizontal Sliding in Commensurate Two-Dimensional Homojunctions, *J. Phys. Chem. Lett.*, 2020, **11**, 5815–5822.
5 A. K. Geim, Graphene: Status and Prospects, *Science*, 2009, **324**, 1530–1535.
6 H. Zhang, Ultrathin Two-Dimensional Nanomaterials, *ACS Nano*, 2015, **9**, 9451–9469.
7 S. Z. Butler, S. M. Hollen, L. Cao, Y. Cui, J. A. Gupta, H. R. Gutiérrez, T. F. Heinz, S. S. Hong, J. Huang, A. F. Ismach, E. Johnston-Halperin, M. Kuno, V. V. Plashnitsa, R. D. Robinson, R. S. Ruoff, S. Salahuddin, J. Shan, L. Shi, M. G. Spencer, M. Terrones, W. Windl and J. E. Goldberger, Progress, challenges, and opportunities in two-dimensional materials beyond graphene, *ACS Nano*, 2013, **7**, 2898–2926.
8 M. Nasilowski, B. Mahler, E. Lhuillier, S. Ithurria and B. Dubertret, Two-Dimensional Colloidal Nanocrystals, *Chem. Rev.*, 2016, **116**, 10934–10982.
9 Y. Chen, Z. Fan, Z. Zhang, W. Niu, C. Li, N. Yang, B. Chen and H. Zhang, Two-Dimensional Metal Nanomaterials: Synthesis, Properties, and Applications, *Chem. Rev.*, 2018, **118**, 6409–6455.
10 C. S. Ah, Y. J. Yun, H. J. Park, W. J. Kim, D. H. Ha and W. S. Yun, Size-controlled synthesis of machinable single crystalline gold nanoplates, *Chem. Mater.*, 2005, **17**, 5558–5561.
11 Q. Zhang, N. Li, J. Goebl, Z. Lu and Y. Yin, A systematic study of the synthesis of silver nanoplates: Is citrate a 'magic' reagent?, *J. Am. Chem. Soc.*, 2011, **133**, 18931–18939.
12 Z. Li and X. Peng, Size/shape-controlled synthesis of colloidal CdSe quantum disks: Ligand and temperature effects, *J. Am. Chem. Soc.*, 2011, **133**, 6578–6586.
13 S. Pedetti, B. Nadal, E. Lhuillier, B. Mahler, C. Bouet, B. Abécassis, X. Xu and B. Dubertret, Optimized synthesis of CdTe nanoplatelets and photoresponse of CdTe nanoplatelets films, *Chem. Mater.*, 2013, **25**, 2455–2462.
14 L. F. Klepzig, L. Biesterfeld, M. Romain, A. Niebur, A. Schlosser, J. Hübner and J. Lauth, Colloidal 2D PbSe nanoplatelets with efficient emission reaching the telecom O-, E- and S-band, *Nanoscale Adv.*, 2022, **4**, 590–599.
15 N. Saenz, L. S. Hamachi, A. Wolock, B. H. Goodge, A. Kuntzmann, B. Dubertret, I. Billinge, L. F. Kourkoutis, D. A. Muller, A. C. Crowther and J. S. Owen, Synthesis of graded $CdS_{1-x}Se_x$ nanoplatelet alloys and heterostructures from pairs of chalcogenoureas with tailored conversion reactivity, *Chem. Sci.*, 2023, **14**, 12345–12354.
16 A. G. Rachkov and A. M. Schimpf, Colloidal Synthesis of Tunable Copper Phosphide Nanocrystals, *Chem. Mater.*, 2021, **33**, 1394–1406.
17 J. S. Son, M. K. Choi, M. K. Han, K. Park, J. Y. Kim, S. J. Lim, M. Oh, Y. Kuk, C. Park, S. J. Kim and T. Hyeon, N-type nanostructured thermoelectric materials prepared from chemically synthesized ultrathin Bi_2Te_3 nanoplates, *Nano Lett.*, 2012, **12**, 640–647.
18 A. Puthirath Balan, S. Radhakrishnan, C. F. Woellner, S. K. Sinha, L. Deng, C. D. L. Reyes, B. M. Rao, M. Paulose, R. Neupane, A. Apte, V. Kochat, R. Vajtai, A. R. Harutyunyan, C. W. Chu, G. Costin, D. S. Galvao, A. A. Martí, P. A. Van Aken, O. K. Varghese, C. S. Tiwary, A. Malie Madom Ramaswamy Iyer and P. M. Ajayan, Exfoliation of a non-van der Waals material from iron ore hematite, *Nat. Nanotechnol.*, 2018, **13**, 602–609.
19 K. Zhu, Y. Tao, D. E. Clark, W. Hong and C. W. Li, Solution-Phase Synthesis of Vanadium Intercalated 1T′-WS_2 with Tunable Electronic Properties, *Nano Lett.*, 2023, **23**, 4471–4478.
20 K. Zhu, Y. Tao, S. Mandal, M. Chen and C. W. Li, Factors Controlling Intercalation of Metal Atoms into WS_2: Implications for Electronically Tunable Semiconductors, *ACS Appl. Nano Mater.*, 2023, **6**, 16846–16855.
21 M. Yang, G. Cheng, N. Mathur, R. Singha, F. Yuan, N. Yao and L. M. Schoop, Chemical exfoliation of 1-dimensional antiferromagnetic nanoribbons from a non-van der Waals material, *Nanoscale Horiz.*, 2024, 479–486.
22 Z. Cai, B. Liu, X. Zou and H. M. Cheng, Chemical Vapor Deposition Growth and Applications of Two-Dimensional Materials and Their Heterostructures, *Chem. Rev.*, 2018, **118**, 6091–6133.
23 J. Yu, J. Li, W. Zhang and H. Chang, Synthesis of high quality two-dimensional materials via chemical vapor deposition, *Chem. Sci.*, 2015, **6**, 6705–6716.
24 T. Alam, B. Wang, R. Pulavarthy, M. A. Haque, C. Muratore, N. Glavin, A. K. Roy and A. A. Voevodin, Domain engineering of physical vapor deposited two-dimensional materials, *Appl. Phys. Lett.*, 2014, **105**, 21.
25 C. Muratore, J. J. Hu, B. Wang, M. A. Haque, J. E. Bultman, M. L. Jespersen, P. J. Shamberger, M. E. McConney, R. D. Naguy and A. A. Voevodin, Continuous ultra-thin MoS_2 films grown by low-temperature physical vapor deposition, *Appl. Phys. Lett.*, 2014, **104**, 1–6.
26 J. Zhou, Q. Zeng, D. Lv, L. Sun, L. Niu, W. Fu, F. Liu, Z. Shen, C. Jin and Z. Liu, Controlled Synthesis of High-Quality Monolayered α-In_2Se_3 via Physical Vapor Deposition, *Nano Lett.*, 2015, **15**, 6400–6405.
27 A. G. Rachkov, K. Chalek, H. Yin, M. Xu, G. P. Holland and A. M. Schimpf, Redox Chemistries for Vacancy Modulation in Plasmonic Copper Phosphide Nanocrystals, *ACS Nano*, 2024, **18**(7), 5282–5296.
28 B. Mahler, V. Hoepfner, K. Liao and G. A. Ozin, Colloidal synthesis of 1T-WS_2 and 2H-WS_2 nanosheets: Applications for photocatalytic hydrogen evolution, *J. Am. Chem. Soc.*, 2014, **136**, 14121–14127.
29 Y. Yan, B. Xia, X. Ge, Z. Liu, J. Y. Wang and X. Wang, Ultrathin MoS_2 nanoplates with rich active sites as highly efficient catalyst for hydrogen evolution, *ACS Appl. Mater. Interfaces*, 2013, **5**, 12794–12798.

30 W. Shi, L. Zhou, S. Song, J. Yang and H. Zhang, Hydrothermal synthesis and thermoelectric transport properties of impurity-free antimony telluride hexagonal nanoplates, *Adv. Mater.*, 2008, **20**, 1892–1897.
31 Y. Xu, Z. Ren, W. Ren, G. Cao, K. Deng and Y. Zhong, Hydrothermal synthesis of single-crystalline Bi_2Te_3 nanoplates, *Mater. Lett.*, 2008, **62**, 4273–4276.
32 X. Fan, P. Xu, Y. C. Li, D. Zhou, Y. Sun, M. A. T. Nguyen, M. Terrones and T. E. Mallouk, Controlled Exfoliation of MoS_2 Crystals into Trilayer Nanosheets, *J. Am. Chem. Soc.*, 2016, **138**, 5143–5149.
33 N. Liu, P. Kim, J. H. Kim, J. H. Ye, S. Kim and C. J. Lee, Large-area atomically thin MoS_2 nanosheets prepared using electrochemical exfoliation, *ACS Nano*, 2014, **8**, 6902–6910.
34 J. Dong, L. Liu, C. Tan, Q. Xu, J. Zhang, Z. Qiao, D. Chu, Y. Liu, Q. Zhang, J. Jiang, Y. Han, A. P. Davis and Y. Cui, Free-standing homochiral 2D monolayers by exfoliation of molecular crystals, *Nature*, 2022, **602**, 606–611.
35 H. Peng, S. Meister, C. K. Chan, X. F. Zhang and Y. Cui, Morphology control of layer-structured gallium selenide nanowires, *Nano Lett.*, 2007, **7**, 199–203.
36 M. Lin, D. Wu, Y. Zhou, W. Huang, W. Jiang, W. Zheng, S. Zhao, C. Jin, Y. Guo, H. Peng and Z. Liu, Controlled growth of atomically thin In_2Se_3 flakes by van der Waals epitaxy, *J. Am. Chem. Soc.*, 2013, **135**, 13274–13277.
37 Y. Li, J. Zhang, G. Zheng, Y. Sun, S. S. Hong, F. Xiong, S. Wang, H. R. Lee and Y. Cui, Lateral and Vertical Two-Dimensional Layered Topological Insulator Heterostructures, *ACS Nano*, 2015, **9**, 10916–10921.
38 M. Aagesen, E. Johnson, C. B. Sørensen, S. O. Mariager, R. Feidenhans'l, E. Spiecker, J. Nygård and P. E. Lindelof, Molecular beam epitaxy growth of free-standing plane-parallel InAs nanoplates, *Nat. Nanotechnol.*, 2007, **2**, 761–764.
39 Z. Wu, E. Mu, Z. Wang, X. Chen, Z. Wu, Y. Liu and Z. Hu, Bi_2Te_3 Nanoplates' Selective Growth Morphology on Different Interfaces for Enhancing Thermoelectric Properties, *Cryst. Growth Des.*, 2019, **19**(7), 3639–3646.
40 K. P. Loh, S. M. Poh, X. Zhao, S. J. Rong Tan, D. Fu, W. Fei, L. Chu, D. Jiadong, W. Zhou, S. J. Pennycook and A. H. Castro Neto, Molecular beam epitaxy of highly crystalline $MoSe_2$ on hexagonal boron nitride, *ACS Nano*, 2018, **12**, 7562–7570.
41 E. Lhuillier, S. Pedetti, S. Ithurria, B. Nadal, H. Heuclin and B. Dubertret, Two-Dimensional colloidal metal chalcogenides semiconductors: Synthesis, spectroscopy, and applications, *Acc. Chem. Res.*, 2015, **48**, 22–30.
42 Y. Sun, M. Terrones and R. E. Schaak, Colloidal Nanostructures of Transition-Metal Dichalcogenides, *Acc. Chem. Res.*, 2021, **54**, 1517–1527.
43 P. D. Cunningham, I. Coropceanu, K. Mulloy, W. Cho and D. V. Talapin, Quantized Reaction Pathways for Solution Synthesis of Colloidal ZnSe Nanostructures: A Connection between Clusters, Nanowires, and Two-Dimensional Nanoplatelets, *ACS Nano*, 2020, **14**, 3847–3857.
44 B. T. Diroll, D. V. Talapin and R. D. Schaller, Violet-to-Blue Gain and Lasing from Colloidal CdS Nanoplatelets: Low-Threshold Stimulated Emission Despite Low Photoluminescence Quantum Yield, *ACS Photonics*, 2017, **4**, 576–583.
45 I. Fedin and D. V. Talapin, Colloidal CdSe Quantum Rings, *J. Am. Chem. Soc.*, 2016, **138**, 9771–9774.
46 C. She, I. Fedin, D. S. Dolzhnikov, P. D. Dahlberg, G. S. Engel, R. D. Schaller and D. V. Talapin, Red, Yellow, Green, and Blue Amplified Spontaneous Emission and Lasing Using Colloidal CdSe Nanoplatelets, *ACS Nano*, 2015, **9**, 9475–9485.
47 F. Fievet, J. P. Lagier, B. Blin, B. Beaudoin and M. Figlarz, Homogeneous and heterogeneous nucleations in the polyol process for the preparation of micron and submicron size metal particles, *Solid State Ionics*, 1989, **32–33**, 198–205.
48 F. Fievet, S. Ammar-Merah, R. Brayner, F. Chau, M. Giraud, F. Mammeri, J. Peron, J. Y. Piquemal, L. Sicard and G. Viau, The polyol process: a unique method for easy access to metal nanoparticles with tailored sizes, shapes and compositions, *Chem. Soc. Rev.*, 2018, **47**, 5187–5233.
49 S. E. Skrabalak, B. J. Wiley, M. Kim, E. V. Formo and Y. Xia, On the polyol synthesis of silver nanostructures: Glycolaldehyde as a reducing agent, *Nano Lett.*, 2008, **8**, 2077–2081.
50 H. Yue, Y. Zhao, X. Ma and J. Gong, Ethylene glycol: Properties, synthesis, and applications, *Chem. Soc. Rev.*, 2012, **41**, 4218–4244.
51 J. H. Lee, K. Kamada, N. Enomoto and J. Hojo, Polyhedral gold nanoplate: High fraction synthesis of two-dimensional nanoparticles through rapid heating process, *Cryst. Growth Des.*, 2008, **8**, 2638–2645.
52 C. Li, W. Cai, B. Cao, F. Sun, Y. Li, C. Kan and L. Zhang, Mass synthesis of large, single-crystal Au nanosheets based on a polyol process, *Adv. Funct. Mater.*, 2006, **16**, 83–90.
53 H. Liu and Q. Yang, A two-step temperature-raising process to gold nanoplates with optical and surface enhanced Raman spectrum properties, *CrystEngComm*, 2011, **13**, 2281–2288.
54 Z. Guo, Y. Zhang, Y. DuanMu, L. Xu, S. Xie and N. Gu, Facile synthesis of micrometer-sized gold nanoplates through an aniline-assisted route in ethylene glycol solution, *Colloids Surf., A*, 2006, **278**, 33–38.
55 T. Tang and I. W. Hamley, Multiple morphologies of gold nano-plates by high-temperature polyol syntheses, *Colloids Surf., A*, 2009, **336**, 1–7.
56 D. Seo, C. Il Yoo, I. S. Chung, S. M. Park, S. Ryu and H. Song, Shape adjustment between multiply twinned and single-crystalline polyhedral gold nanocrystals: Decahedra, icosahedra, and truncated tetrahedra, *J. Phys. Chem. C*, 2008, **112**, 2469–2475.
57 Y. Xiong, A. R. Siekkinen, J. Wang, Y. Yin, M. J. Kim and Y. Xia, Synthesis of silver nanoplates at high yields by

slowing down the polyol reduction of silver nitrate with polyacrylamide, *J. Mater. Chem.*, 2007, **17**, 2600–2602.

58 Z. Liu, H. Zhou, Y. S. Lim, J. H. Song, L. Piao and S. H. Kim, Synthesis of silver nanoplates by two-dimensional oriented attachment, *Langmuir*, 2012, **28**, 9244–9249.

59 C. W. Chang, F. C. Lin, C. Y. Chiu, C. Y. Su, J. S. Huang, T. P. Perng and T. J. Yen, HNO_3-assisted polyol synthesis of ultralarge single-crystalline Ag microplates and their far propagation length of surface plasmon polariton, *ACS Appl. Mater. Interfaces*, 2014, **6**, 11791–11798.

60 D. Köhler, M. Heise, A. I. Baranov, Y. Luo, D. Geiger, M. Ruck and M. Armbrüster, Synthesis of BiRh nanoplates with superior catalytic performance in the semihydrogenation of acetylene, *Chem. Mater.*, 2012, **24**, 1639–1644.

61 W. Z. Wang, B. Poudel, Y. Ma and Z. F. Ren, Shape control of single crystalline bismuth nanostructures, *J. Phys. Chem. B*, 2006, **110**, 25702–25706.

62 C. Kan, X. Zhu and G. Wang, Single-crystalline gold microplates: Synthesis, characterization, and thermal stability, *J. Phys. Chem. B*, 2006, **110**, 4651–4656.

63 Y. Xiong, J. M. McLellan, J. Chen, Y. Yin, Z. Y. Li and Y. Xia, Kinetically controlled synthesis of triangular and hexagonal nanoplates of palladium and their SPR/SERS properties, *J. Am. Chem. Soc.*, 2005, **127**, 17118–17127.

64 Y. Zhang, M. E. Grass, S. E. Habas, F. Tao, T. Zhang, P. Yang and G. A. Somorjai, One-step polyol synthesis and langmuir-blodgett monolayer formation of size-tunable monodisperse rhodium nanocrystals with catalytically active (111) surface structures, *J. Phys. Chem. C*, 2007, **111**, 12243–12253.

65 L. Scarabelli, M. Sun, X. Zhuo, S. Yoo, J. E. Millstone, M. R. Jones and L. M. Liz-Marzán, Plate-Like Colloidal Metal Nanoparticles, *Chem. Rev.*, 2023, **123**, 3493–3542.

66 X. K. Gu, B. Liu and J. Greeley, First-Principles Study of Structure Sensitivity of Ethylene Glycol Conversion on Platinum, *ACS Catal.*, 2015, **5**, 2623–2631.

67 B. Liu and J. Greeley, A density functional theory analysis of trends in glycerol decomposition on close-packed transition metal surfaces, *Phys. Chem. Chem. Phys.*, 2013, **15**, 6475–6485.

68 H. Hao, D. Sun, Y. Xu, P. Liu, G. Zhang, Y. Sun and D. Gao, Hematite nanoplates: Controllable synthesis, gas sensing, photocatalytic and magnetic properties, *J. Colloid Interface Sci.*, 2016, **462**, 315–324.

69 F. X. Ma, P. P. Wang, C. Y. Xu, J. Yu, H. T. Fang and L. Zhen, Synthesis of self-stacked $CuFe_2O_4$-Fe_2O_3 porous nanosheets as a high performance Li-ion battery anode, *J. Mater. Chem. A*, 2014, **2**, 19330–19337.

70 H. Han, Y. Ni and E. Sheng, ZnO nanoplates assembled by rod-like nanoparticles: simple reflux synthesis, influential factors and shape evolution towards nanorings, *RSC Adv.*, 2015, **5**, 51750–51761.

71 L. Liu, Z. Yang, H. Liang, H. Yang and Y. Yang, Shape-controlled synthesis of manganese oxide nanoplates by a polyol-based precursor route, *Mater. Lett.*, 2010, **64**, 891–893.

72 N. N. Sinha and N. Munichandraiah, Single-Shot Preparation of Crystalline Nanoplate $LiFePO_4$ by a Simple Polyol Route, *J. Electrochem. Soc.*, 2010, **157**, A824.

73 H. J. Zhu, X. M. Liu, H. Yang and X. D. Shen, Effect of the stirring rate on physical and electrochemical properties of $LiMnPO_4$ nanoplates prepared in a polyol process, *Ceram. Int.*, 2014, **40**, 6699–6704.

74 J. Li, R. Yao and C. Cao, $LiNi_{1/3}Co_{1/3}Mn_{1/3}O_2$ Nanoplates with {010} Active Planes Exposing Prepared in Polyol Medium as a High-Performance Cathode for Li-Ion Battery, *ACS Appl. Mater. Interfaces*, 2014, **6**, 5075–5082.

75 W. Xu, F. Lyu, Y. Bai, A. Gao, J. Feng, Z. Cai and Y. Yin, Porous cobalt oxide nanoplates enriched with oxygen vacancies for oxygen evolution reaction, *Nano Energy*, 2018, **43**, 110–116.

76 Z. Liu, R. Ma, M. Osada, K. Takada and T. Sasaki, Selective and controlled synthesis of α- and β-cobalt hydroxides in highly developed hexagonal platelets, *J. Am. Chem. Soc.*, 2005, **127**, 13869–13874.

77 Y. Liu, M. Calcabrini, Y. Yu, S. Lee, C. Chang, J. David, T. Ghosh, M. C. Spadaro, C. Xie, O. Cojocaru-Mirédin, J. Arbiol and M. Ibáñez, Defect Engineering in Solution-Processed Polycrystalline SnSe Leads to High Thermoelectric Performance, *ACS Nano*, 2022, **16**, 78–88.

78 R. J. Mehta, Y. Zhang, C. Karthik, B. Singh, R. W. Siegel, T. Borca-Tasciuc and G. Ramanath, A new class of doped nanobulk high-figure-of-merit thermoelectrics by scalable bottom-up assembly, *Nat. Mater.*, 2012, **11**, 233–240.

79 L. S. Hamachi, H. Yang, I. Jen-La Plante, N. Saenz, K. Qian, M. P. Campos, G. T. Cleveland, I. Rreza, A. Oza, W. Walravens, E. M. Chan, Z. Hens, A. C. Crowther and J. S. Owen, Precursor reaction kinetics control compositional grading and size of $CdSe_{1-x}S_x$ nanocrystal heterostructures, *Chem. Sci.*, 2019, **10**, 6539–6552.

80 E. Bennett, M. W. Greenberg, A. J. Jordan, L. S. Hamachi, S. Banerjee, S. J. L. Billinge and J. S. Owen, Size Dependent Optical Properties and Structure of ZnS Nanocrystals Prepared from a Library of Thioureas, *Chem. Mater.*, 2022, **34**, 706–717.

81 S. Kang, D. Lee, J. Kim, A. Capasso, H. S. Kang, J. W. Park, C. H. Lee and G. H. Lee, 2D semiconducting materials for electronic and optoelectronic applications: Potential and challenge, *2D Mater.*, 2020, **7**, 2.

82 J. P. Heremans, R. J. Cava and N. Samarth, Tetradymites as thermoelectrics and topological insulators, *Nat. Rev. Mater.*, 2017, **2**, 17049.

83 D. Jing and L. Guo, A novel method for the preparation of a highly stable and active CdS photocatalyst with a special surface nanostructure, *J. Phys. Chem. B*, 2006, **110**, 11139–11145.

84 H. Li, X. Wang, J. Xu, Q. Zhang, Y. Bando, D. Golberg, Y. Ma and T. Zhai, One-dimensional CdS nanostructures: A promising candidate for optoelectronics, *Adv. Mater.*, 2013, **25**, 3017–3037.

85 L. Cheng, Q. Xiang, Y. Liao and H. Zhang, CdS-Based photocatalysts, *Energy Environ. Sci.*, 2018, **11**, 1362–1391.
86 J. Deb, R. Majidi and U. Sarkar, Bilayer CdS Structure: A Promising Candidate for Photocatalytic and Optoelectronic Applications, *ACS Appl. Opt. Mater.*, 2023, **1**, 201–208.
87 X. Wang, M. Liu, Z. Zhou and L. Guo, Toward Facet Engineering of CdS Nanocrystals and Their Shape-Dependent Photocatalytic Activities, *J. Phys. Chem. C*, 2015, **119**, 20555–20560.
88 Z. Li, H. Chen, Y. Li, H. Wang, Y. Liu, X. Li, H. Lin, S. Li and L. Wang, Porous direct Z-scheme heterostructures of S-deficient CoS/CdS hexagonal nanoplates for robust photocatalytic H_2 generation, *CrystEngComm*, 2022, **24**, 404–416.
89 X. Leng, Y. Wang and F. Wang, Alcohols Assisted Hydrothermal Synthesis of Defect-Rich MoS_2 and Their Applications in Humidity Sensing, *Adv. Mater. Interfaces*, 2019, **6**, 1–11.
90 H. Wang and D. C. Zou, Polyol-mediated synthesis of MoS_2 nanosheets using sulfur powder as the sulfur source, *Acta Phys.-Chim. Sin.*, 2017, **33**, 1027–1032.
91 Q. Zhang, K. Yu, B. Zhao, Y. Wang, C. Song, S. Li, H. Yin, Z. Zhang and Z. Zhu, Synthesis of a MoS_2@MWNT nanostructure with enhanced field emission and electrochemical properties, *RSC Adv.*, 2013, **3**, 10994–11000.
92 Y. Zhu, L. Peng, W. Zhu, D. Akinwande and G. Yu, Layer-by-Layer Assembly of Two-Dimensional Colloidal Cu_2Se Nanoplates and Their Layer-Dependent Conductivity, *Chem. Mater.*, 2016, **28**, 4307–4314.
93 H. Liu, J. Zhang, X. Zheng, G. Liu, H. Hu, W. Pan, C. Liu, Q. Hao and H. Chen, Polyol process synthesis of metal selenide nanomaterials and their photovoltaic application, *CrystEngComm*, 2016, **18**, 6860–6866.
94 W. Fu, M. Liu, F. Xue, X. Wang, Z. Diao and L. Guo, Facile polyol synthesis of CuS nanocrystals with a hierarchical nanoplate structure and their application for electrocatalysis and photocatalysis, *RSC Adv.*, 2016, **6**, 80361–80367.
95 A. Datta, D. Mukherjee, S. Witanachchi and P. Mukherjee, Low temperature synthesis, optical and photoconductance properties of nearly monodisperse thin In_2S_3 nanoplatelets, *RSC Adv.*, 2013, **3**, 141–147.
96 M. S. Mahdi, K. Ibrahim, A. Hmood, N. M. Ahmed, S. A. Azzez and F. I. Mustafa, A highly sensitive flexible SnS thin film photodetector in the ultraviolet to near infrared prepared by chemical bath deposition, *RSC Adv.*, 2016, **6**, 114980–114988.
97 Y. M. Han, J. Zhao, M. Zhou, X. X. Jiang, H. Q. Leng and L. F. Li, Thermoelectric performance of SnS and SnS-SnSe solid solution, *J. Mater. Chem. A*, 2015, **3**, 4555–4559.
98 Z. Guo, Y. Xie, J. Xiao, Z. Zhao, Y. Wang, Z. Xu, Y. Zhang, L. Yin, H. Cao and J. Gong, High thermoelectric performance in low-cost $SnS_{0.91}Se_{0.09}$ crystals, *Science*, 2019, **80**, 1418–1424.
99 J. Chao, Z. Wang, X. Xu, Q. Xiang, W. Song, G. Chen, J. Hu and D. Chen, Tin sulfide nanoribbons as high performance photoelectrochemical cells, flexible photodetectors and visible-light-driven photocatalysts, *RSC Adv.*, 2013, **3**, 2746–2753.
100 Z. Lin, Y. Chen, A. Yin, Q. He, X. Huang, Y. Xu, Y. Liu, X. Zhong, Y. Huang and X. Duan, Solution processable colloidal nanoplates as building blocks for high-performance electronic thin films on flexible substrates, *Nano Lett.*, 2014, **14**, 6547–6553.
101 X. Yan, W. Zheng, F. Liu, S. Yang and Z. Wang, Thickness Effects for Thermoelectric Property of Antimony Telluride Nanoplatelets via Solvothermal Method, *Sci. Rep.*, 2016, **6**, 37722.
102 H. Q. Yang, L. Miao, C. Y. Liu, C. Li, S. Honda, Y. Iwamoto, R. Huang and S. Tanemura, A Facile Surfactant-Assisted Reflux Method for the Synthesis of Single-Crystalline Sb_2Te_3 Nanostructures with Enhanced Thermoelectric Performance, *ACS Appl. Mater. Interfaces*, 2015, **7**, 14263–14271.
103 T. Q. Kimberly, K. M. Ciesielski, X. Qi, E. S. Toberer and S. M. Kauzlarich, High Thermoelectric Performance in 2D Sb_2Te_3 and Bi_2Te_3 Nanoplate Composites Enabled by Energy Carrier Filtering and Low Thermal Conductivity, *ACS Appl. Electron. Mater.*, 2024, **6**(5), 2816–2825.
104 B. Zhou, Y. Ji, Y. F. Yang, X. H. Li and J. J. Zhu, Rapid microwave-assisted synthesis of single-crystalline Sb_2Te_3 hexagonal nanoplates, *Cryst. Growth Des.*, 2008, **8**, 4394–4397.
105 G. H. Dong, Y. J. Zhu and L. D. Chen, Microwave-assisted rapid synthesis of Sb_2Te_3 nanosheets and thermoelectric properties of bulk samples prepared by spark plasma sintering, *J. Mater. Chem.*, 2010, **20**, 1976–1981.
106 Y. Min, J. W. Roh, H. Yang, M. Park, S. Il Kim, S. Hwang, S. M. Lee, K. H. Lee and U. Jeong, Surfactant-free scalable synthesis of Bi_2Te_3 and Bi_2Se_3 nanoflakes and enhanced thermoelectric properties of Their Nanocomposites, *Adv. Mater.*, 2013, **25**, 1425–1429.
107 Z. Li, R. Teng, S. Zheng, Y. Zhang, T. Huang and G. Lu, Single-crystalline Bi_2Te_3 nanosheets with uniform morphology via a simple, efficient, and high-yield microwave-assisted synthesis, *J. Cryst. Growth*, 2014, **406**, 104–110.
108 G. Zhang, W. Wang, X. Lu and X. Li, Solvothermal synthesis of V-VI binary and ternary hexagonal platelets: the oriented attachment mechanism, *Cryst. Growth Des.*, 2009, **9**, 145–150.
109 C. Dun, C. A. Hewitt, Q. Jiang, Y. Guo, J. Xu, Y. Li, Q. Li, H. Wang and D. L. Carroll, Bi_2Te_3 Plates with Single Nanopore: The Formation of Surface Defects and Self-Repair Growth, *Chem. Mater.*, 2018, **30**, 1965–1970.
110 T. Q. Kimberly, E. Y. C. Wang, G. D. Navarro, X. Qi, K. M. Ciesielski, E. S. Toberer and S. M. Kauzlarich, Into the Void: Single Nanopore in Colloidally Synthesized Bi_2Te_3 Nanoplates with Ultralow Lattice Thermal Conductivity, *Chem. Mater.*, 2024, **36**, 6618–6626.
111 Y. Liu, Y. Zhang, K. H. Lim, M. Ibáñez, S. Ortega, M. Li, J. David, S. Martí-Sánchez, K. M. Ng, J. Arbiol, M. V. Kovalenko, D. Cadavid and A. Cabot, High

Thermoelectric Performance in Crystallographically Textured n-Type $Bi_2Te_{3-x}Se_x$ Produced from Asymmetric Colloidal Nanocrystals, *ACS Nano*, 2018, **12**, 7174–7184.

112 M. Zeng, H. Xie, M. Saeidi-Javash, A. Tanvir, Y. Du, J. Chen, M. G. Kanatzidis and Y. Zhang, Scalable nanomanufacturing of chalcogenide inks: a case study on thermoelectric V-VI nanoplates, *J. Mater. Chem. A*, 2021, **9**, 22555–22562.

113 M. Hong, T. C. Chasapis, Z. G. Chen, L. Yang, M. G. Kanatzidis, G. J. Snyder and J. Zou, N-Type $Bi_2Te_{3-x}Se_x$ Nanoplates with Enhanced Thermoelectric Efficiency Driven by Wide-Frequency Phonon Scatterings and Synergistic Carrier Scatterings, *ACS Nano*, 2016, **10**, 4719–4727.

114 Z. Ju, Y. Hou, A. Bernard, V. Taufour, D. Yu and S. M. Kauzlarich, Ambipolar Topological Insulator and High Carrier Mobility in Solution Grown Ultrathin Nanoplates of Sb-Doped Bi_2Se_3, *ACS Appl. Electron. Mater.*, 2019, **1**, 1917–1923.

115 L. X. Liang, Y. Deng, Y. Wang and H. L. Gao, Epitaxial formation of core-shell heterostructured Bi_2Te_3@Sb_2Te_3 hexagonal nanoplates, *J. Nanopart. Res.*, 2014, **16**, 1.

116 F. Fei, Z. Wei, Q. Wang, P. Lu, S. Wang, Y. Qin, D. Pan, B. Zhao, X. Wang, J. Sun, X. Wang, P. Wang, J. Wan, J. Zhou, M. Han, F. Song, B. Wang and G. Wang, Solvothermal Synthesis of Lateral Heterojunction Sb_2Te_3/Bi_2Te_3 Nanoplates, *Nano Lett.*, 2015, **15**, 5905–5911.

117 Y. Min, G. Park, B. Kim, A. Giri, J. Zeng, J. W. Roh, S. II Kim, K. H. Lee and U. Jeong, Synthesis of Multishell Nanoplates by Consecutive Epitaxial Growth of Bi_2Se_3 and Bi_2Te_3 Nanoplates and Enhanced Thermoelectric Properties, *ACS Nano*, 2015, **9**(7), 6843–6853.

118 Z. Lin, A. Yin, J. Mao, Y. Xia, N. Kempf, Q. He, Y. Wang, C. Y. Chen, Y. Zhang, V. Ozolins, Z. Ren, Y. Huang and X. Duan, Scalable solution-phase epitaxial growth of symmetry-mismatched heterostructures on two-dimensional crystal soft template, *Sci. Adv.*, 2016, **2**, 1–10.

119 Z. Ju, C. Crawford, J. Adamczyk, E. S. Toberer and S. M. Kauzlarich, Study of the Thermoelectric Properties of Bi_2Te_3/Sb_2Te_3 Core-Shell Heterojunction Nanostructures, *ACS Appl. Mater. Interfaces*, 2022, **14**, 24886–24896.

120 C. Bauer, I. Veremchuk, C. Kunze, A. Benad, V. M. Dzhagan, D. Haubold, D. Pohl, G. Schierning, K. Nielsch, V. Lesnyak and A. Eychmüller, Heterostructured Bismuth Telluride Selenide Nanosheets for Enhanced Thermoelectric Performance, *Small Sci.*, 2021, **1**, 2000021.

121 Y. W. Zhang, X. Sun, R. Si, L. P. You and C. H. Yan, Single-crystalline and monodisperse LaF_3 triangular nanoplates from a single-source precursor, *J. Am. Chem. Soc.*, 2005, **127**, 3260–3261.

122 Y. P. Du, X. Sun, Y. W. Zhang, Z. G. Yan, L. D. Sun and C. H. Yan, Uniform alkaline earth fluoride nanocrystals with diverse shapes grown from thermolysis of metal trifluoroacetates in hot surfactant solutions, *Cryst. Growth Des.*, 2009, **9**, 2013–2019.

123 A. Singh, Y. C. Chen, K. C. Wu, S. M. Peng, T. R. Kuo and D. Y. Wang, Kinetic Studies of Oleylamine-Based 2D-Lead Bromide Perovskite with Controllable n-Value by Sequential Addition of Cesium at Room Temperature, *J. Phys. Chem. C*, 2023, **127**, 14839–14846.

124 A. Sarkar, P. Acharyya, R. Sasmal, P. Pal, S. S. Agasti and K. Biswas, Synthesis of Ultrathin Few-Layer 2D Nanoplates of Halide Perovskite $Cs_3Bi_2I_9$ and Single-Nanoplate Super-Resolved Fluorescence Microscopy, *Inorg. Chem.*, 2018, **57**, 15558–15565.

125 Q. A. Akkerman, S. G. Motti, A. R. Srimath Kandada, E. Mosconi, V. D'Innocenzo, G. Bertoni, S. Marras, B. A. Kamino, L. Miranda, F. De Angelis, A. Petrozza, M. Prato and L. Manna, Solution Synthesis Approach to Colloidal Cesium Lead Halide Perovskite Nanoplatelets with Monolayer-Level Thickness Control, *J. Am. Chem. Soc.*, 2016, **138**, 1010–1016.

126 R. Qin, H. Song, G. Pan, X. Bai, B. Dong, S. Xie, L. Liu, Q. Dai, X. Qu, X. Ren and H. Zhao, Polyol-mediated synthesis of hexagonal LaF_3 nanoplates using $NaNO_3$ as a mineralizer, *Cryst. Growth Des.*, 2009, **9**, 1750–1756.

127 X. Qu, H. K. Yang, J. W. Chung, B. K. Moon, B. C. Choi, J. H. Jeong and K. H. Kim, Polyol-mediated solvothermal synthesis and luminescence properties of CeF_3, and CeF_3:Tb^{3+} nanocrystals, *J. Solid State Chem.*, 2011, **184**, 246–251.

128 Y. Xu, D. Chen, X. Jiao and L. Ba, PEG-assisted fabrication of single-crystalline CuI nanosheets: A general route to two-dimensional nanostructured materials, *J. Phys. Chem. C*, 2007, **111**, 6–9.

129 A. Manthiram, An Outlook on Lithium Ion Battery Technology, *ACS Cent. Sci.*, 2017, **3**, 1063–1069.

130 P. Ganguly, M. Harb, Z. Cao, L. Cavallo, A. Breen, S. Dervin, D. D. Dionysiou and S. C. Pillai, 2D Nanomaterials for Photocatalytic Hydrogen Production, *ACS Energy Lett.*, 2019, **4**, 1687–1709.

131 G. Zhuang, J. Yan, Y. Wen, Z. Zhuang and Y. Yu, Two-Dimensional Transition Metal Oxides and Chalcogenides for Advanced Photocatalysis: Progress, Challenges, and Opportunities, *Sol. RRL*, 2021, **5**, 1–50.

132 X. Zhang, H. Li, S. Wang, F. R. F. Fan and A. J. Bard, Improvement of hematite as photocatalyst by doping with tantalum, *J. Phys. Chem. C*, 2014, **118**, 16842–16850.

133 Y. Li, Z. Li, C. Chi, H. Shan, L. Zheng and Z. Fang, Plasmonics of 2D Nanomaterials: Properties and Applications, *Adv. Sci.*, 2017, **4**, 1–25.

134 A. Elbanna, H. Jiang, Q. Fu, J. F. Zhu, Y. Liu, M. Zhao, D. Liu, S. Lai, X. W. Chua, J. Pan, Z. X. Shen, L. Wu, Z. Liu, C. W. Qiu and J. Teng, 2D Material Infrared Photonics and Plasmonics, *ACS Nano*, 2023, **17**, 4134–4179.

135 I. T. Witting, T. C. Chasapis, F. Ricci, M. Peters, N. A. Heinz, G. Hautier and G. J. Snyder, The Thermoelectric Properties of Bismuth Telluride, *Adv. Electron. Mater.*, 2019, **5**, 1800904.